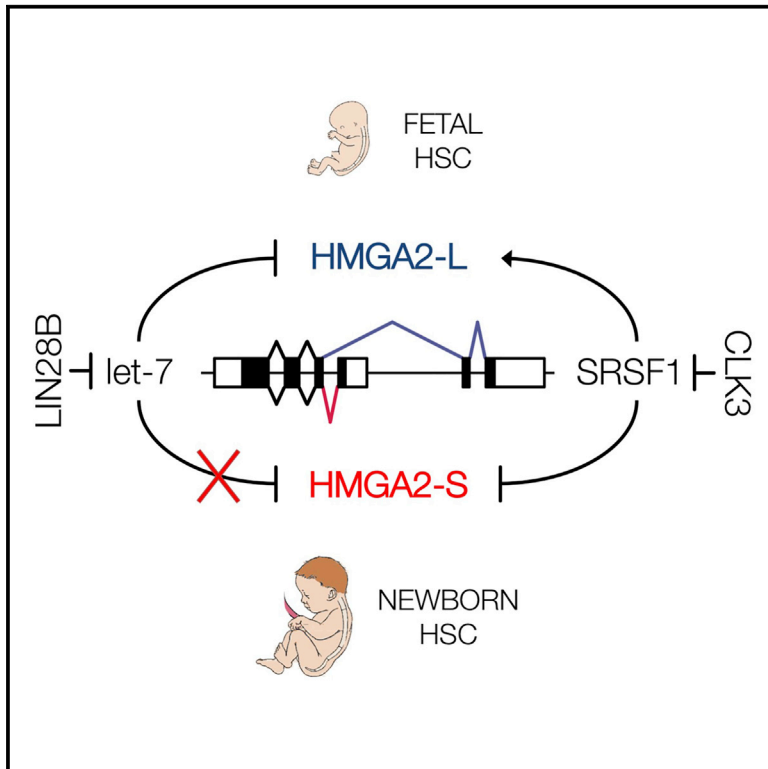


Cell Stem Cell

A CLK3-HMGA2 Alternative Splicing Axis Impacts Human Hematopoietic Stem Cell Molecular Identity throughout Development

Graphical Abstract



Authors

Marcella Cesana, Michael H. Guo, Davide Cacchiarelli, ..., Alexander Meissner, Joel N. Hirschhorn, George Q. Daley

Correspondence

george.daley@childrens.harvard.edu

In Brief

Human hematopoietic stem cells (HSCs) display substantial transcriptional diversity during development. Here, we investigated the contribution of alternative splicing to such diversity by analyzing the dynamics of a key hematopoietic regulator, HMGA2. Next, we showed that CLK3, by regulating the splicing pattern of *HMGA2*, reinforces an HSC-specific program.

Highlights

- Substantial diversity of human HSC transcriptomes shown at distinct developmental stages
- HMGA2 alternative 3' UTR usage is functional to avoid miRNA-mediated inhibition
- CLK3 affects the HMGA2 splicing pattern by promoting exon skipping



A CLK3-HMGA2 Alternative Splicing Axis Impacts Human Hematopoietic Stem Cell Molecular Identity throughout Development

Marcella Cesana,^{1,2,3,18} Michael H. Guo,^{4,5,6,7,18} Davide Cacchiarelli,^{3,4,8,9,10,18} Lara Wahlster,^{1,2,3} Jessica Barragan,^{1,2,3} Sergei Doulatov,¹¹ Linda T. Vo,^{1,2,3} Beatrice Salvatori,¹² Cole Trapnell,¹³ Kendall Clement,^{3,4,8} Patrick Cahan,¹⁴ Kaloyan M. Tsanov,^{1,2,3} Patricia M. Sousa,^{1,2,3} Barbara Tazon-Vega,^{3,4,8} Adriano Bolondi,¹ Federico M. Giorgi,¹² Andrea Califano,^{12,15} John L. Rinn,^{3,4,8,16} Alexander Meissner,^{3,4,8,17} Joel N. Hirschhorn,^{4,5,6,7} and George Q. Daley^{1,2,3,19,*}

¹Stem Cell Program, Division of Hematology/Oncology, Manton Center for Orphan Disease Research, Boston Children's Hospital and Dana-Farber Cancer Institute, Boston, MA 02115, USA

²Department of Biological Chemistry and Molecular Pharmacology, Harvard Stem Cell Institute, Harvard Medical School, Boston, MA 02115, USA

³Harvard Stem Cell Institute, Cambridge, MA 02138, USA

⁴Broad Institute of MIT and Harvard, Cambridge, MA 02142, USA

⁵Division of Endocrinology, Boston Children's Hospital, Boston, MA 02115, USA

⁶Center for Basic and Translational Obesity Research, Boston Children's Hospital, Boston, MA 02115, USA

⁷Department of Genetics, Harvard Medical School, Boston, MA 02115, USA

⁸Department of Stem Cell and Regenerative Biology, Harvard University, Cambridge, MA 02138, USA

⁹Telethon Institute of Genetics and Medicine (TIGEM), Armenise/Harvard Laboratory of Integrative Genomics, Pozzuoli 80078, Italy

¹⁰Department of Translational Medicine, University of Naples "Federico II", Naples 80131, Italy

¹¹Division of Hematology, University of Washington, Seattle, WA 98195, USA

¹²Department of Systems Biology, Columbia University, New York, NY 10032, USA

¹³Department of Genome Sciences, University of Washington, Seattle, WA 98115, USA

¹⁴Department of Biomedical Engineering, Institute for Cell Engineering, Johns Hopkins University School of Medicine, Baltimore, MD 21205, USA

¹⁵Departments of Biomedical Informatics, Biochemistry and Molecular Biophysics, JP Sulzberger Columbia Genome Center, Herbert Irving Comprehensive Cancer Center, Columbia University, New York, NY 10032, USA

¹⁶University of Colorado Boulder Biofrontiers, Boulder, CO 80301, USA

¹⁷Max Planck Institute for Molecular Genetics, 14195 Berlin, Germany

¹⁸These authors contributed equally

¹⁹Lead Contact

*Correspondence: george.daley@childrens.harvard.edu

<https://doi.org/10.1016/j.stem.2018.03.012>

SUMMARY

While gene expression dynamics have been extensively cataloged during hematopoietic differentiation in the adult, less is known about transcriptome diversity of human hematopoietic stem cells (HSCs) during development. To characterize transcriptional and post-transcriptional changes in HSCs during development, we leveraged high-throughput genomic approaches to profile miRNAs, lincRNAs, and mRNAs. Our findings indicate that HSCs manifest distinct alternative splicing patterns in key hematopoietic regulators. Detailed analysis of the splicing dynamics and function of one such regulator, *HMGA2*, identified an alternative isoform that escapes miRNA-mediated targeting. We further identified the splicing kinase *CLK3* that, by regulating *HMGA2* splicing, preserves *HMGA2* function in the setting of an increase in *let-7* miRNA levels, delineating how *CLK3* and *HMGA2* form a functional axis that influences HSC properties during development. Collectively, our study high-

lights molecular mechanisms by which alternative splicing and miRNA-mediated post-transcriptional regulation impact the molecular identity and stage-specific developmental features of human HSCs.

INTRODUCTION

Hematopoiesis is the coordinated lineage commitment, differentiation, and expansion of hematopoietic stem cells (HSCs) to generate mature blood cells. Interestingly, hematopoiesis occurs at distinct anatomic sites during development, including the yolk sac and fetal liver during fetal life and bone marrow during post-natal life (Mikkola and Orkin, 2006). While HSCs from these sites are all capable of generating the full complement of mature blood cells, they differ in certain characteristics. For example, several studies have shown that HSCs from earlier developmental zones have higher regenerative capacity (Babovic and Eaves, 2014). Understanding differences in hematopoiesis along development can shed insight on processes important in HSC function and regeneration, with important clinical applications in stem cell transplantation.



Recent research has leveraged high-throughput genomic profiling to characterize the hematopoietic hierarchy at a molecular level (Vedi et al., 2016). Although these studies have generated novel insights into hematopoietic lineage commitment and differentiation, our understanding of the molecular and functional differences among developmentally distinct HSC populations remains inadequate. Murine studies have begun to address this gap (Cabezas-Wallscheid et al., 2014; McKinney-Freeman et al., 2012), but, owing to species-specific differences (Doulatov et al., 2012), emerging efforts are starting to characterize the molecular diversity along the human hematopoietic hierarchy (Notta et al., 2016; Novershtern et al., 2011).

The generation and tuning of expression of alternative splicing isoforms can contribute to significant transcriptional diversity (Wang et al., 2008). However, studies are just beginning to delineate their involvement in hematopoiesis (Chen et al., 2014; Rentas et al., 2016). The discovery that core spliceosomal proteins and accessory regulatory splicing factors are frequently mutated in various hematopoietic malignancies (Sperling et al., 2017; Yoshida et al., 2011) has further spurred research into the regulation and role of alternative splicing during normal hematopoiesis (Chen et al., 2014; Crews et al., 2016; Wong et al., 2013).

Here, we dissect the transcriptional identity of human HSCs from multiple developmental stages and establish developmental stage-specific expression signatures. Through integrative analyses, we then describe how alternative splicing and microRNA (miRNA)-mediated post-transcriptional regulation interplay to regulate HSC identity.

RESULTS

Transcriptional Diversity in Human HSCs across Ontogeny

Fetal liver (FL), umbilical cord blood (CB), and bone marrow (BM) represent distinct progressive stages of hematopoiesis during development. To dissect transcriptional features of human HSC populations, we prospectively isolated immunophenotypically defined early HSCs (CD34⁺ CD38⁻ CD90⁺ CD45RA⁻) from FL, CB, and BM, as well as corresponding committed CD34⁺CD38⁺ progenitor populations (PROG). We performed RNA sequencing (RNA-seq) and miRNA profiling (Figure 1A).

Transitions from FL to CB and from CB to BM HSCs were marked by substantial changes in gene expression (2,469 and 1,572 genes, respectively; false discovery rate [FDR] < 0.01) (Figure 1B, left). While recent studies have highlighted several hallmark genes for HSC identity (e.g., *HOXA9*, *LMO2*, *MECOM*; (Ebina and Rossi, 2015), our results suggest that they are in fact highly dynamic across HSC populations, with a limited set of genes uniformly expressed across HSC populations (e.g., *HLF*, *PRDM16*—Figure S1A and Table S1). Additionally, our analysis highlights several factors not intrinsic to HSCs, such as genes from the niche in which HSCs develop (e.g., liver genes like *KDR* and *FCN2* in FL-HSCs) and genes involved in blood pressure regulation (e.g., *AVP* in CB-HSCs, Figure S1B).

RNA-processing events generate splicing isoforms that vary across cell types, contribute extensively to functional diversity (Wang et al., 2008), and have been implicated in hematopoietic

aging and leukemia pathogenesis (Crews et al., 2016). Thus, we expanded our analysis to examine the transcriptional landscape at the isoform level (Trapnell et al., 2012). We detected a large number of genes (215 in CB versus FL, 105 in CB versus BM; FDR < 0.01), including key regulators *HMGA2*, *DNMT1*, and *MEIS1*, that were differentially expressed among HSC populations at the isoform level but displayed little to no differential expression at the gene level (Figure 1B, right, and Table S1). We also refined the isoform-level analysis by examining differential usage of 5' UTRs, 3' UTRs, coding sequences (CDS), and transcriptional start sites (TSS) (Figure S1C, related to Figure 1B).

Based on the observed transcriptional diversity, we generated a map of stage-specific mRNAs and lincRNAs, isoforms, and miRNAs (Figure 1C and Tables S2A and S2B). As an illustration, we highlight *PROM1*, previously implicated in stem cell biology (Miraglia et al., 1997). We detected six isoforms of *PROM1*, which display distinct expression patterns across HSCs. In particular, we detected isoforms with differential inclusion of exon 3, which encodes for part of the core prominin domain (Figures 1D and S1D).

To further understand the alternative splicing patterns in HSC populations, we performed pairwise percent spliced-in (PSI) analyses of exons among the HSC populations (Alamancos et al., 2015). We examined different splicing events, including alternative 5' splice site (A5), alternative 3' splice site (A3), alternative first exon (AF), alternative last exon (AL), mutually exclusive exon (MX), retained intron (RI), and skipping exon (SE) (Figure 1E). Interestingly, there appeared to be an increase in RI events along HSC development from FL to CB and to BM-HSCs (both $p < 0.05$).

Given the important roles for lincRNAs in stem cells (Fatica and Bozzoni, 2014), we performed *de novo* lincRNA discovery from the RNA-seq data. We identified 6905 lincRNAs, 76 of which were differentially expressed among HSC and PROG populations, suggesting that lincRNAs contribute to transcriptional diversity of HSCs (Figure 1C, middle, and Table S2A). *MEG3*, an HSC-specific lincRNA implicated in maintenance of LT-HSC function (Qian et al., 2016), displayed a developmentally regulated expression pattern (Figure 1F).

Analysis of miRNA expression uncovered additional transcriptome diversity (Figure 1C, bottom, and Table S2B). For example, *let-7* family members and *miR-126* are highly expressed across HSCs (together accounting for as much as 20% of the total measured miRNA content) but demonstrate a developmentally regulated expression pattern (Figure 1G).

To understand the function of the differentially expressed genes, we applied gene set enrichment analysis (GSEA) to examine enrichment among curated gene sets (Figure 1H). FL-HSCs were enriched for “cell-cycle” and “checkpoints” signatures. In contrast, CB-HSCs were enriched in “RNA metabolism” and “3'-UTR-mediated translational regulation” pathways. Broad expression of target genes of known transcriptional regulators (“MYC targets,” “EZH2 targets”) were also observed among different HSC populations.

Together, these analyses defined developmental-stage specific molecular signatures for each HSC population that reflect substantial transcriptional diversity at the gene and isoform levels and which is also present in noncoding RNAs.

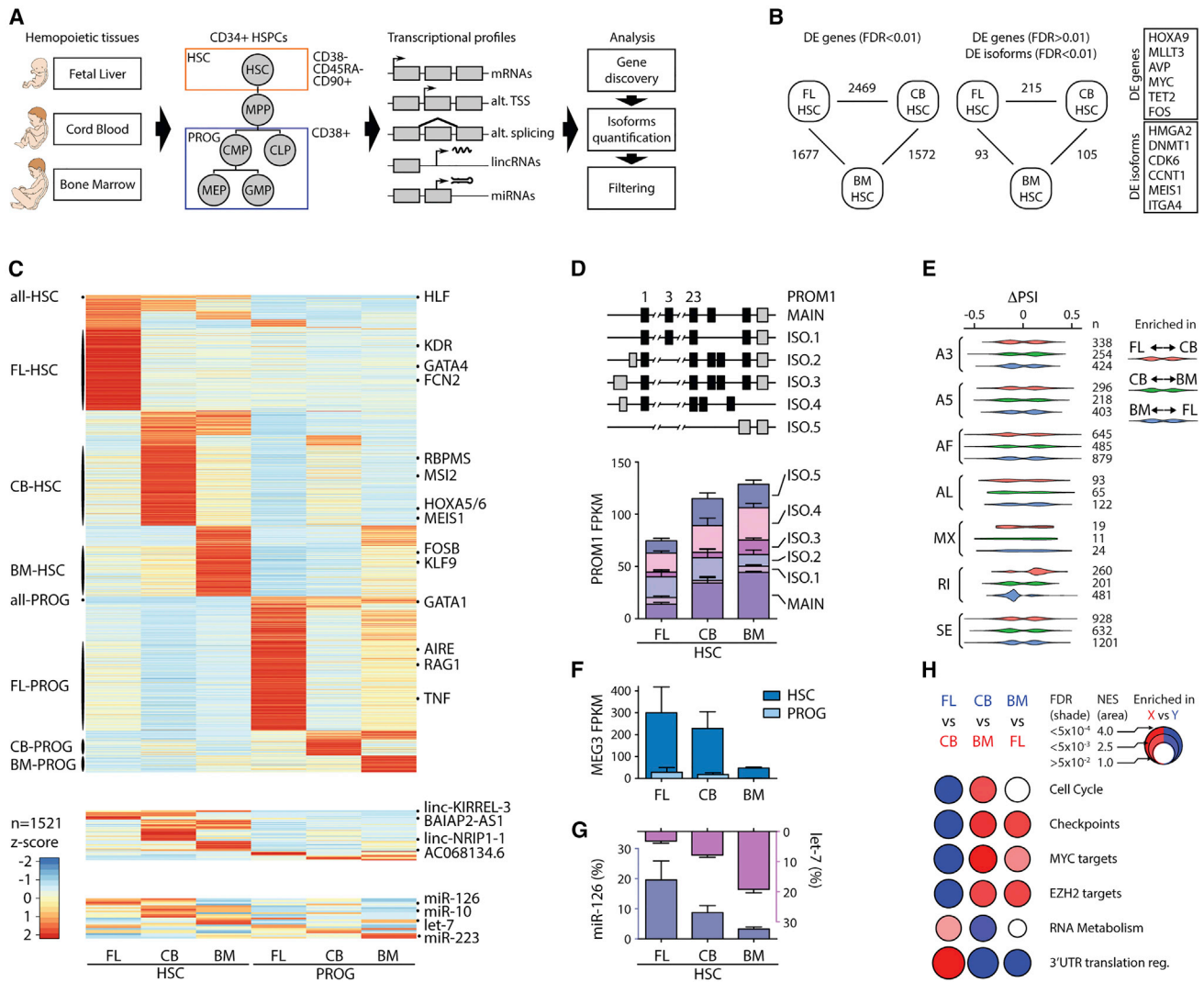


Figure 1. Transcriptional Diversity among Human HSCs along Development

(A) Schematic representation of fluorescence-activated cell sorting (FACS) and transcriptomic analyses. Hematopoietic stem cells (HSC) and progenitor (PROG) cells were isolated according to the indicated surface markers from human fetal liver (FL), umbilical cord blood (CB), and bone marrow (BM) CD34⁺ cells. RNA sequencing of both coding (mRNAs) and noncoding RNAs (lincRNAs) was performed along with miRNA expression quantification.

(B) (left) Pairwise comparisons showing the number of differentially expressed (DE) genes at FDR < 0.01. (right) DE transcripts at isoform level (FDR < 0.01), but not at gene level (FDR > 0.01). Representative genes for each category are shown on the right. The full dataset can be found in Table S1.

(C) Expression heatmap of DE mRNA isoforms (top), lincRNAs (middle), and miRNAs (bottom). Representative isoforms shared among all HSC types (all-HSC) or progenitors (all-PROG), or specific to each population (as listed on left) are indicated on the right. The full dataset can be found in Table S2.

(D) (top) Gene structure of the most highly expressed *PROM1* isoforms (ISO) detected by RNA-seq. (bottom) Bar plot showing *PROM1* expression (in FPKM) in the indicated HSC samples. Reference exon numbers are listed on top (constitutive exons are not shown), with coding exons in black and UTRs in gray.

(E) Violin plot representing distributions of statistically significant Δ PSI values ($p < 0.05$) for different classes of PSI events: alternative 3' splice site (A3), alternative 5' splice site (A5), alternative first exon (AF), alternative last exon (AL), mutually exclusive exon (MX), retained intron (RI), and skipping exon (SE). Separate violins are shown for each pairwise comparison of HSC samples, and the number of events in each violin are shown on the right. Δ PSI values are shown for the second sample as compared to the first sample in each pair.

(F) *MEG3* lincRNA expression quantification by RNA-seq (in FPKM) in HSC and PROG samples.

(G) Bar plot showing expression of *let-7* family members (purple) and *miR-126* (blue) in HSCs. Expression is shown as the percentage of total measured miRNA counts for each HSC population.

(H) BubbleMap visualization (Spinelli et al., 2015) of representative gene set enrichment analysis (GSEA) results between pairs of HSC samples. As indicated in the legend, for each GO category, colors (red versus blue) correspond to the sample label, shades represent statistical significance (FDR), and the area of the circle represents the enrichment (normalized enrichment score, NES). Empty circles correspond to non-significant enrichments (FDR > 0.05). The full dataset can be found in Table S4.

Mean \pm SD values are shown for (D), (F), and (G). FPKM, fragments per kilobase of transcript per million mapped reads.

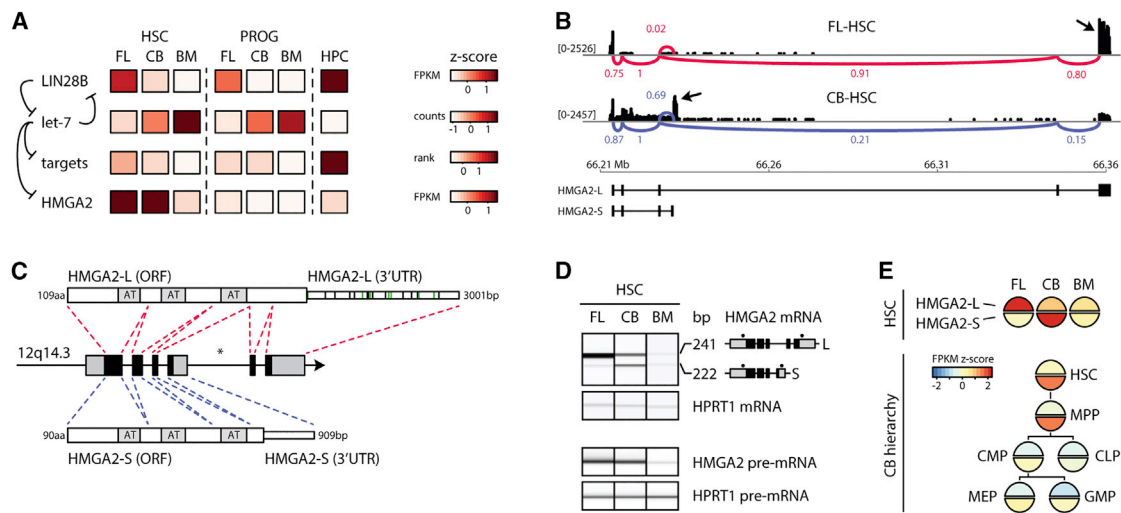


Figure 2. HMGGA2 Alternative Splicing in Human HSCs

(A) Heatmap showing expression of *LIN28B*, *let-7* family members, the ranked median expression of the top 100 predicted *let-7* targets, and *HMGGA2*. Previously dissected regulatory relationships of the *LIN28*-*let-7*-*HMGGA2* pathway (Viswanathan et al., 2008) are indicated with arrows. Scales are shown on the right as normalized Z scores.

(B) Visualization of RNA-seq reads (black bars) mapping at *HMGGA2* (drawn to scale) in the indicated samples. A sashimi plot displaying the major splice junctions (FL-HSCs, red; CB-HSCs, blue) is superimposed. The abundance of each splicing junction is indicated and is normalized to the counts for the shared exon 2–3 splice junction (with value of 1). Arrows indicate the reads mapping to the terminal exons that distinguish the *HMGGA2*-L and *HMGGA2*-S isoforms.

(C) Structure of the human *HMGGA2* locus (not drawn to scale). In the middle, locus coordinates are indicated along with coding exons (black) and UTRs (gray). Asterisk indicates location of major chromosomal rearrangements detected in malignancies (Kazmierczak et al., 1996). Red and blue dashed lines indicate how exons are spliced to result in *HMGGA2*-L (top) and *HMGGA2*-S (bottom). Gray boxes indicate the AT-binding hook domains. Green and black slashes indicate predicted binding sites of *let-7* family members and other conserved HSC-expressed miRNAs, respectively.

(D) (Top) Digital gel from RT-PCR electropherogram showing expression of *HMGGA2*-L and *HMGGA2*-S from the indicated HSC populations. Sizes of the amplicons are indicated on the right, along with the structure of each isoform (coding exons in black, UTRs in gray) and the position of the primers used for PCR co-amplification (black dots). (Bottom) Digital gel from RT-PCR electropherogram showing expression of *HMGGA2* pre-mRNA from the indicated HSC populations. *HPRT1* was used as the control for both gels. Expression levels of *HMGGA2* isoforms are indicated in Figure S2 and Table S2A.

(E) Shaded circles show *HMGGA2* isoform expression (Z-score-normalized FPKM values) across HSCs and CB hierarchy from publicly available data (Stunnenberg et al., 2016). MPP, multipotent progenitors; CMP, common myeloid progenitors; MEP, myeloid erythroid progenitors; GMP, granulocyte macrophage progenitors; CLP, common lymphoid progenitors.

Identification of an HSC Stage-Specific *HMGGA2* Isoform

Our analyses identified a number of transcripts differentially expressed at the isoform level but not at the gene level (Figure 1B, and Table S1). These include key HSC regulators whose differential expression patterns were previously undetected with gene-level analyses. Among the most differentially expressed was an isoform of *HMGGA2* (ENST00000403681.2) in the transition from FL- to CB-HSCs (>5-fold decrease, FDR < 0.01), but which remained relatively unchanged at the gene level (FDR > 0.9) (Table S1). *HMGGA2* is a component of the *LIN28*-*let-7* axis that regulates development (Shyh-Chang and Daley, 2013). Consistent with *LIN28*'s role in inhibiting *let-7* biogenesis (Viswanathan et al., 2008), we observed a gradual decrease of *LIN28B* during maturation from FL- to BM-HSCs, with a concomitant increase in levels of *let-7* family members (Figure 2A). Hematopoietic progenitor cells (HPCs) derived from *in vitro* differentiation of induced pluripotent stem cells (iPSC) displayed the highest levels of *LIN28B* and lowest levels of *let-7* members, reflecting their embryonic nature (Chadwick et al., 2003). More broadly, we observed that the expression of the top 100 *in silico*-predicted *let-7* targets (Agarwal et al., 2015) were inversely correlated with expression of *let-7* (Figure 2A).

HMGGA2, a well-characterized target of *let-7* (Lee and Dutta, 2007), was surprisingly discordant in expression with respect to *let-7*. *HMGGA2* was highly expressed in both CB- and FL-HSCs, despite *let-7* levels being higher in CB as compared to FL-HSCs (Figure 2A). RNA-seq results highlighted a complex splicing pattern with at least four *HMGGA2* isoforms expressed in HSCs (Figures S2A and S2B). Quantitative visualization of the RNA-seq reads revealed that the canonical full-length isoform (ENST00000403681.2; hereafter named *HMGGA2*-L) is highly expressed in FL-HSCs, while CB-HSCs show high expression of a shorter isoform (ENST00000393578.3; hereafter named *HMGGA2*-S) (Figure 2B). *HMGGA2*-L and *HMGGA2*-S share the first three exons but differ in their terminal exon usage (including C-terminal domains and 3' UTRs) (Figures 2C and S2A). Notably, the *HMGGA2*-S 3' UTR is only one-third the length of the *HMGGA2*-L 3' UTR and is devoid of most of the conserved miRNA sites, including the seven experimentally validated *let-7* sites (May et al., 2007) (Figure 2C). Semiquantitative PCR confirmed the expression patterns of *HMGGA2*-L and *HMGGA2*-S isoforms (Figure 2D, top). Moreover, *HMGGA2* pre-mRNA levels were high and comparable in FL- and CB-HSCs, before decreasing in BM-HSCs, suggesting that in the transition between CB- to BM-HSCs, *HMGGA2* expression is likely downregulated at the

transcriptional rather than post-transcriptional level (Figure 2D, bottom). Global analyses identified several other genes that in the HSC developmental transitions display a different major isoform with a distinct 3' UTR devoid of *let-7* binding sites (Table S3).

Using public data from the Blueprint Epigenome Project (Stunnenberg et al., 2016), we investigated expression of *HMGA2-L* and *HMGA2-S* in six stem and progenitor cell populations derived from the CB hierarchy (Figure 2E, bottom). *HMGA2-S* is detectable at high levels in HSCs and in multipotent progenitors. Conversely, *HMGA2-L* is expressed at low levels across these same six CB-derived hematopoietic populations, consistent with our data (Figure 2E, top).

Genome-wide Mapping of *HMGA2* Isoform Chromatin Binding

HMGA2 is an architectural transcription factor, binding chromatin broadly to help recruit other transcription factors and regulate gene expression (Ozturk et al., 2014). To determine whether the proteins encoded by the *HMGA2* isoforms have different functions, we evaluated *HMGA2* chromatin occupancy genome-wide by performing isoform-specific chromatin immunoprecipitation sequencing (ChIP-seq) in two hematopoietic cell types: K562 cells and conditionally immortalized iPSC-derived hematopoietic progenitors (HPC-5F) (Doulatov et al., 2013). These cells were selected for their variable expression of endogenous *HMGA2* (Fragments Per Kilobase Million reads [FPKM] = 0 in K562; FPKM = 44 in HPC-5F) (Uhlén et al., 2015).

We used lentiviral constructs containing V5-tagged *HMGA2-L* (L-V5) and *HMGA2-S* (S-V5) open reading frame (ORF) to infect K562 and HPC-5F cells. Both V5 (Figure 3A) and *HMGA2* (data not shown) antibodies immunoprecipitated a large amount of DNA upon overexpression (O/E) of either construct. ChIP-seq of the immunoprecipitate from HPC-5F revealed that, unlike the H3K4me2 profile, *HMGA2* binding is broad, as recently shown (Colombo et al., 2017), and that *HMGA2-L* and *HMGA2-S* proteins display comparable binding patterns (Figure 3B). Ontology analysis revealed that loci with high *HMGA2-L* and *HMGA2-S* binding are enriched for genes related to cell cycle, DNA, and RNA metabolism (Figure S3A).

Although *HMGA2* binds broadly across the genome, we identified promoter regions with the highest and the lowest level of *HMGA2* binding (see STAR Methods). We observed that promoters with the highest *HMGA2-L* or *HMGA2-S* binding were also marked by high H3K4me2 levels (V5 Hi - K4 Hi - Figure 3C). We also observed that highly expressed genes are skewed toward higher *HMGA2* binding at their promoters (Figure S3B). Additionally, within promoters that were enriched for *HMGA2* binding (V5 Hi), we observed an A/T bias (Figure 3D), consistent with *in vitro* observations (Winter et al., 2011). Overall, a strong correlation of binding patterns was observed for *HMGA2-L* and *HMGA2-S* for the most enriched and depleted promoter regions ($r^2 = 0.99$ Figure 3E).

HMGA2 Promotes Expression of HSC-Specific Genes and Enhances Engraftment Capacity

To examine the effects of the two isoforms on downstream gene expression, we performed RNA-seq from HPC-5F transduced with either *HMGA2-L* or *HMGA2-S* ORFs, or control vector (CTRL). A high correlation in downstream gene expression

was observed between *HMGA2-L* and *HMGA2-S* treatments ($r^2 = 0.95$, Figures 3F and S3C). HPC-5F cells have been previously shown to partially reactivate an HSC signature and to enable short-term engraftment into immunocompromised mice (Doulatov et al., 2013). GSEA revealed that enforced expression of either *HMGA2-L* or *HMGA2-S* ORFs enhanced expression of a broad HSC-specific gene signature (Figure 3G). No significant differences were detected when comparing *HMGA2-L* to *HMGA2-S* treatment. Moreover, we observed enhanced repopulating capacity of HPC-5F cells upon O/E of either *HMGA2-L* or *HMGA2-S* ORFs in immunocompromised mice at 16 weeks (Figure 3H).

Collectively, these results revealed that *HMGA2-L* and *HMGA2-S* proteins, despite differences in their C-terminal domains, are highly comparable in their chromatin binding patterns and ability to induce transcriptional changes. The results also link *HMGA2* function to activation of an HSC-specific program and enhanced self-renewal.

miRNA-Mediated Post-transcriptional Regulation Dictates Differential *HMGA2* Isoform Stability

Since *HMGA2-L* and *HMGA2-S* utilize different 3' UTRs (Figure 2C), we hypothesized that the distinct expression patterns (Figure 2D) of the isoforms between FL- and CB-HSCs could be functional in preventing miRNA-mediated post-transcriptional regulation. To test this, we generated reporter constructs with luciferase fused to either the wild-type *HMGA2-L* 3' UTR (Rluc-3'UTRwt_HMGA2-L), *HMGA2-S* 3' UTR (Rluc-3'UTRwt_HMGA2-S), or to a *HMGA2-L* 3' UTR mutated at all HSC-expressed miRNA binding sites (Rluc-3'UTRmt_HMGA2-L).

We transfected the luciferase reporter constructs into *Dgcr8*-knockout mouse embryonic fibroblasts (MEFs K/O DGCR8), along with seven individual HSC-expressed miRNAs and a scramble control. Knockout of *Dgcr8* prevents endogenous miRNA processing, which isolates the role of each miRNA in the absence of endogenous miRNA activity (Han et al., 2009). Among the seven miRNAs analyzed, we found that *let-7* family members had the strongest repressive effect on luciferase activity of *HMGA2-L* 3' UTR (Figure 4A, left). This effect was reversed upon mutation of binding sites for those miRNAs. Additionally, other HSC-expressed miRNAs also appeared to regulate *HMGA2-L* (Figure 4A, left). Moreover, the activity of the construct containing *HMGA2-S* 3' UTR was higher than that of *HMGA2-L* 3' UTR in the context of most miRNA treatments (Figure 4A, right), indicating that *HMGA2-S* 3' UTR has a higher capacity to escape miRNA-mediated repression.

Having demonstrated that the *HMGA2-L* 3' UTR is regulated by a number of miRNAs, we next evaluated whether miRNA-targeting might drive differential stability of the two *HMGA2* isoforms. We used PC-3 and HPC-5F cells, which display high and low endogenous levels of the identified miRNAs, respectively (Figure 4B). Constructs carrying *HMGA2-L* and *HMGA2-S* ORFs along with their corresponding 3' UTRs were used to infect cells, which were then treated with actinomycin-D for 6 hr to halt transcription allowing us to isolate the effect of mRNA stability. qPCR of the *HMGA2* isoforms revealed that *HMGA2-L*+3'UTRwt was more rapidly destabilized than *HMGA2-S*+3'UTRwt (Figure 4C). Conversely, *HMGA2-L*+3'UTRmt expression remained stable over the time points. Overall, we observed that

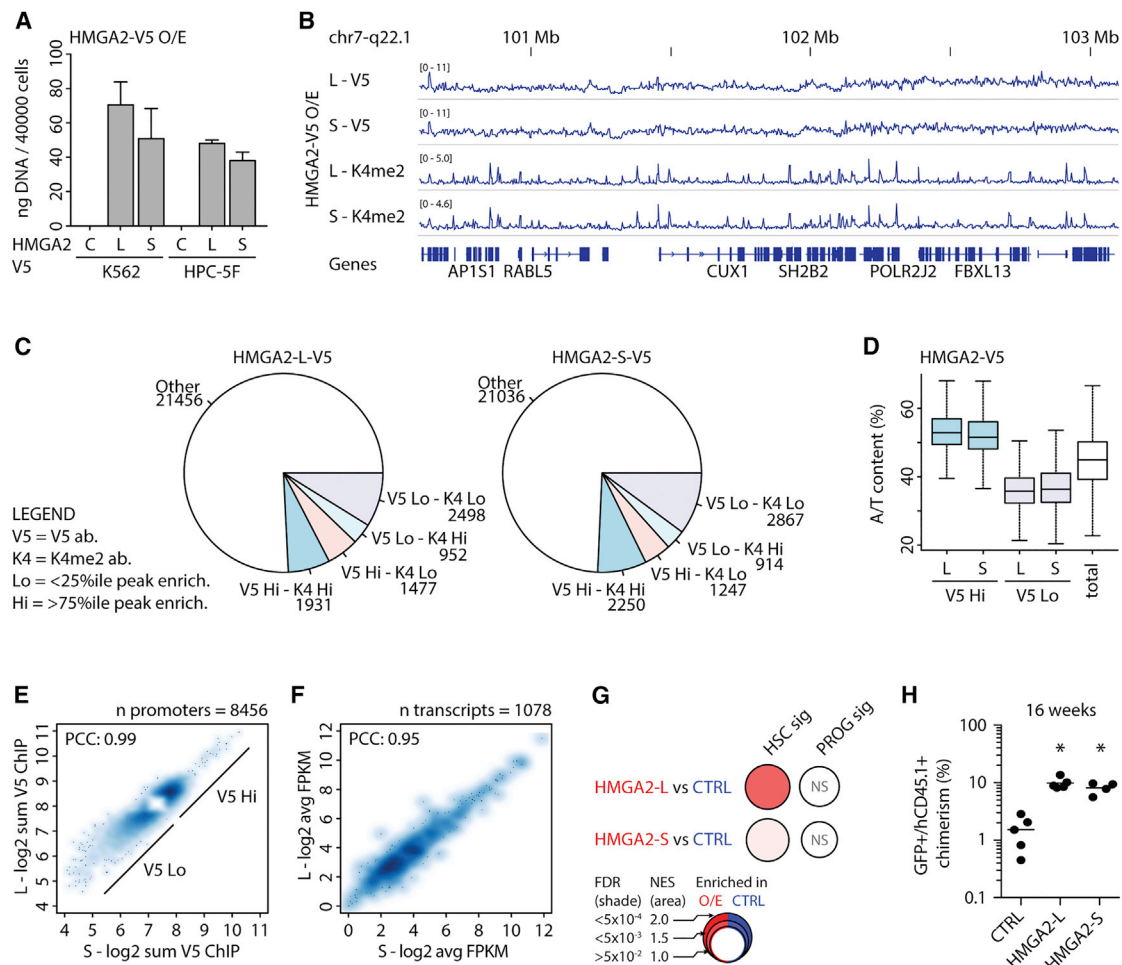


Figure 3. Protein Function of *HMGA2* Isoforms

(A) Amount of DNA immunoprecipitated using V5 antibody in K562 and HPC-5F cells transduced with a control (C) or V5-tagged *HMGA2*-L (L) or *HMGA2*-S (S) ORF lentiviral overexpression (O/E) constructs. Mean \pm SEM values are shown.

(B) Visualization of ChIP-seq read mapping at a sample locus. HPC-5F cells were transduced with V5-tagged *HMGA2*-L or *HMGA2*-S ORF constructs for overexpression of the protein coding regions of the respective isoforms (L or S). ChIP-seq profiles are shown for tagged-*HMGA2* (V5) or H3K4me2 (K4me2). Genes at the locus are indicated on the bottom.

(C) Number of gene promoters (total $n = 28,314$) enriched for *HMGA2* (V5) and H3K4me2 (K4) upon overexpression of *HMGA2*-L (*HMGA2*-L-V5) or *HMGA2*-S (*HMGA2*-S-V5) ORFs. Promoters are considered highly enriched (Hi) for V5 or K4 if they rank in the top quartile of normalized read counts or depleted (Lo) if they fall in the bottom quartile.

(D) A/T content (as a percentage) within immunoprecipitated promoter regions in the V5 Hi and V5 Lo categories or total promoter regions (as a background control). First and third quartiles, medians, and interquartile ranges are shown.

(E) *HMGA2*-L and *HMGA2*-S binding enrichment analysis shows 8456 differentially enriched promoters over the background signal. Correlation between *HMGA2*-L (L) and *HMGA2*-S (S)-enriched promoters is shown for V5 Hi and V5 Lo fractions. Values are reported as the log₂ sum of ChIP replicate signals at promoter regions. PCC is Pearson's correlation coefficient (r^2). Enrichment of GO categories from V5 Hi promoters are shown in Figure S3A.

(F) Differential expression analysis identified 1,078 differentially expressed genes between *HMGA2*-L and *HMGA2*-S and control. Correlation in expression between *HMGA2*-L (L) and *HMGA2*-S (S) treatments is shown. Values are reported as log₂ average of FPKM replicates. PCC is Pearson's correlation coefficient (r^2). The full pairwise comparisons are shown in Figure S3C.

(G) BubbleMap visualization (Spinelli et al., 2015) of GSEA results in HPC-5F cells transduced with *HMGA2*-L and *HMGA2*-S ORFs or control (CTRL) vectors. Gene sets were derived from HSC and PROG-specific signatures from Figure 1C (see Table S2C). As indicated in the legend, colors (red versus blue) correspond to the sample label, shades represent statistical significance (FDR), and the area of the circle represents the enrichment (normalized enrichment score, NES). Empty circles correspond to non-significant (NS) enrichments (FDR > 0.05).

(H) Human chimerism as percentage of GFP⁺CD45.1⁺ in the injected femur of xenografted mice 16 weeks after transplantation of HPC-5F cells transduced with lentivirus for *HMGA2*-L ORF, *HMGA2*-S ORF, or CTRL. Individual and mean values are shown. Mann-Whitney test was used individually comparing each indicated sample with respect to CTRL; * $p < 0.05$.

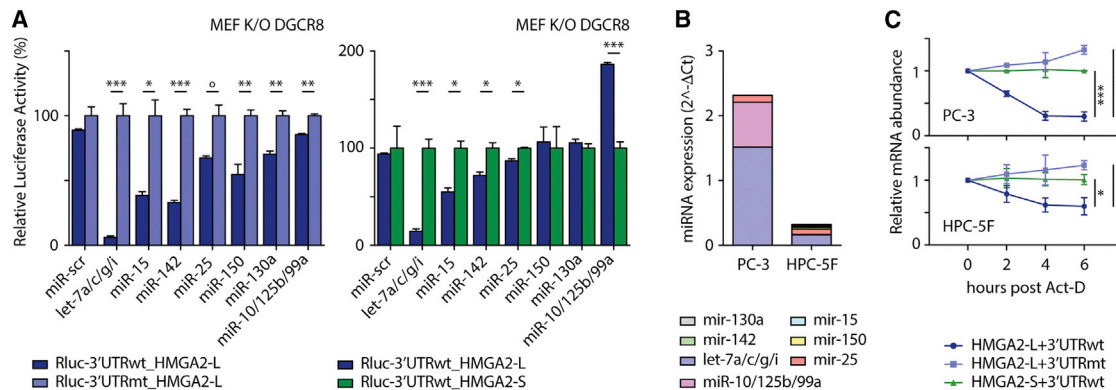


Figure 4. Post-transcriptional Regulation of *HMGA2* Isoforms

(A) Left: Normalized luciferase (Renilla) activity in *Dgcr8*-KO MEF of constructs carrying 3' UTR sequences of *HMGA2*-L (Rluc-3'UTRwt_HMGA2-L) or a mutant derivative depleted for miRNA sites (Rluc-3'UTRmt_HMGA2-L). Right: Normalized luciferase (Renilla) activity in *Dgcr8*-KO MEF of constructs carrying 3' UTR sequences of *HMGA2*-L (Rluc-3'UTRwt_HMGA2-L) or *HMGA2*-S (Rluc-3'UTRwt_HMGA2-S). Normalized luciferase activities were reported with respect to Rluc-3'UTRmt_HMGA2-L (left) or Rluc-3'UTRwt_HMGA2-S (right), set to 100%. Mean \pm SEM values are shown. Unpaired t test was used; * p < 0.05, ** p < 0.01, *** p < 0.005, borderline (\circ = 0.055).

(B) Quantification of miRNAs of interest in PC-3 and HPC-5F cells measured by qRT-PCR. *U6* small nuclear RNA (snRNA) was used as control.

(C) Relative quantification of *HMGA2* isoforms in PC-3 and HPC-5F cells transduced with lentiviral constructs carrying the *HMGA2* ORFs equipped with their corresponding 3' UTRs (HMGA2-L+3'UTRwt and HMGA2-S+3'UTRwt) or a derivative *HMGA2*-L isoform mutated at its miRNA sites (HMGA2-L+3'UTRmt). Infected cells were treated with actinomycin D (Act-D) and harvested at the indicated time points. Expression values were normalized to *HPR1* control and then reported with respect to HMGA2-S+3'UTRwt, set to 1. Mean \pm SEM values are shown. ANOVA was used; * p < 0.05, ** p < 0.01, *** p < 0.005.

HMGA2-L+3'UTRwt destabilization was more pronounced in cells with higher expression of the miRNAs of interest (Figures 4B and 4C).

To demonstrate the regulation of *HMGA2*-L in endogenous settings, we utilized miRNA inhibitors against miRNAs highly expressed in CB-HSCs (*let-7* and *miR-142*, Figure 5B). Consistent with reporter assay results above, inhibition of *let-7* and *miR-142* in CB CD34⁺ cells increased expression of *HMGA2*-L (Figure S4A).

Taken together, these data demonstrate that *HMGA2*-L and *HMGA2*-S isoforms are differentially regulated at the post-transcriptional level and that miRNA levels are critical in determining their stability. These results reconcile the discordant *let-7* and *HMGA2* expression patterns seen in the HSC RNA-seq (Figure 2A). In FL-HSCs, where *HMGA2*-L is the primary isoform (Figure 5A), the cumulative levels of *let-7* and other miRNAs shown to target *HMGA2*-L are the lowest among the HSC populations (Figure 5B). In contrast, in CB-HSCs, where *HMGA2*-S represents the primary isoform (Figure 5A), the expression of these miRNAs was much higher, representing more than 40% of the total measured miRNA content (Figure 5B).

Modulation of *HMGA2* Isoforms Influences Human HSC Function *In Vitro*

To determine whether *HMGA2* isoform dynamics impact HSC properties, we tested their role on human HSC function *in vitro*. We first depleted *HMGA2* using isoform-specific small hairpin RNA (shRNA)-mediated knockdown (KD) in CB CD34⁺ cells (Figure 5C). We designed shRNAs that target only the long (shLONG), short (shSHORT), or both isoforms (shBOTH) (Figure S4B). After 1 week of cytokine-driven serum-free culture, KD of either *HMGA2* isoform in CB CD34⁺ decreased total cell output (data not shown), as well as the CD34⁺CD133⁺CD38⁻

HSC-enriched population (Figure 5D). We also found a reduction in colony-forming potential upon KD of either *HMGA2*-S and *HMGA2*-L (Figure 5E, left). Next, we performed a rescue experiment by co-infecting CB CD34⁺ cells with shBOTH as well as constructs expressing either the *HMGA2*-L and *HMGA2*-S ORFs that bear optimized sequences to escape targeting by shBOTH (see STAR Methods). *HMGA2* ORFs restored colony output of shBOTH-treated CB CD34⁺ cells (Figure 5E, right). Interestingly, we also observed a significant increase of E and GEMM colonies upon *HMGA2* O/E, consistent with the role of *HMGA2* as a positive regulator of erythropoiesis (Copley et al., 2013; Ikeda et al., 2011).

We next evaluated the effect of O/E of each isoform when under the control of its corresponding 3' UTR (Figure 5C). We performed this experiment in primary BM CD34⁺ cells, which have low total *HMGA2* expression (Figure 5A). Cytokine-driven serum-free culture of transduced BM CD34⁺ cells revealed a significant increase in CD34⁺CD133⁺CD38⁻ HSC numbers upon O/E of *HMGA2*-L+3'UTRmt and *HMGA2*-S+3'UTRwt after 1 week of culture (Figure 5F). Forced expression of *HMGA2*-L+3'UTRmt or *HMGA2*-S+3'UTRwt also increased the colony forming potential of transduced BM cells when compared to CTRL. The observed phenotype was more pronounced in *HMGA2*-S+3'UTRwt as compared to *HMGA2*-L+3'UTRmt, with no differences observed in *HMGA2*-L+3'UTRwt-transduced cells (Figure 5G). These results support the functional role of *HMGA2*-S in regulating HSC self-renewal and clonogenic potential capacity *in vitro*.

CLK3 Regulates *HMGA2* Splicing Pattern through SRSF1

We next interrogated the mechanism by which HSCs are able to tune expression of the *HMGA2* isoforms. To do so, we tested splicing regulators for their effect on *HMGA2* isoform expression.

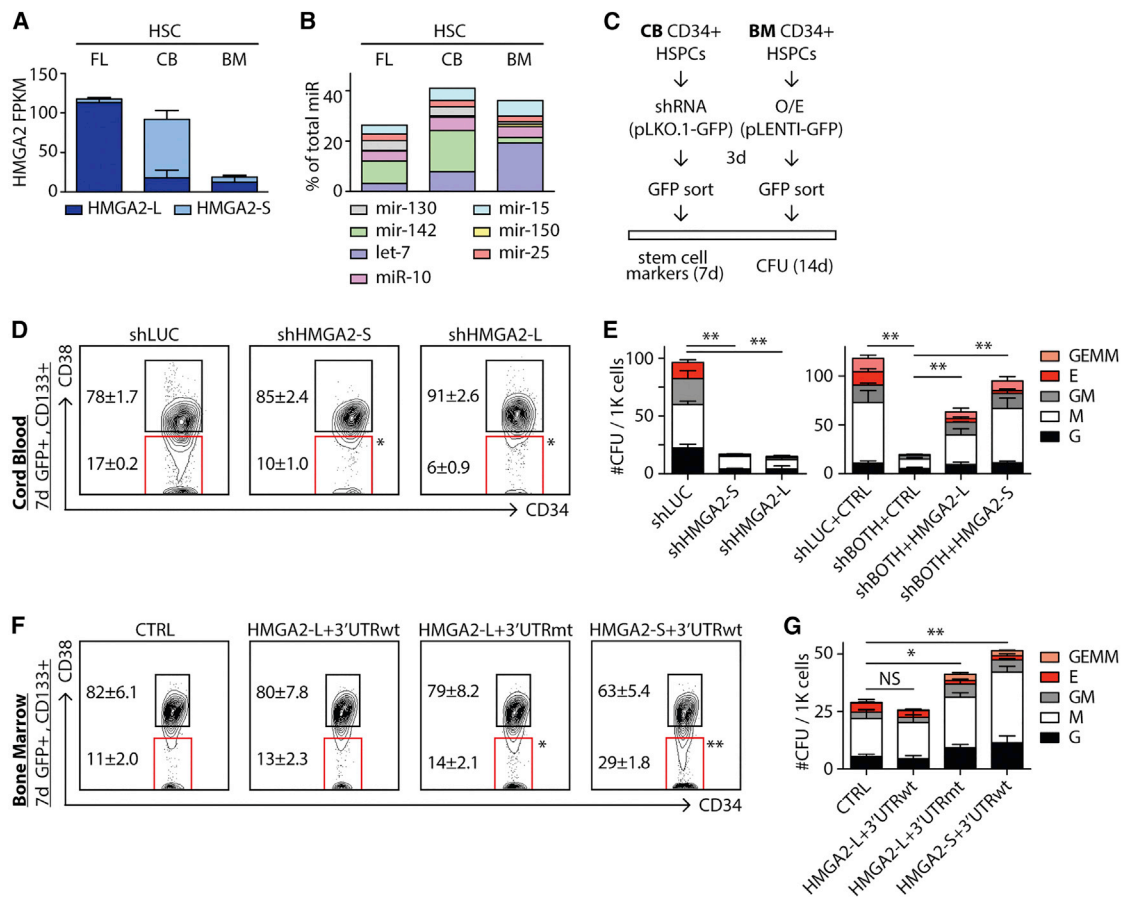


Figure 5. Modulation of *HMGA2* Isoforms in Human HSPCs

(A and B) Absolute expression of the indicated *HMGA2* isoforms (in FPKM) (A) and miRNA families (as percentage of total measured miRNA content) (B) in the indicated HSC populations.

(C) Scheme of *HMGA2* isoform modulation experiments in CB and BM CD34⁺ hematopoietic stem and progenitor cells (HSPCs). Lentiviral constructs (pLKO.1 and pLENTI) also express GFP as a marker to allow for isolation of infected cells.

(D) Phenotypic analysis of the stem cell compartment (CD133⁺CD34⁺CD38⁺) in CB CD34⁺ cells transduced with negative-control hairpin (luciferase-shLUC) or *HMGA2* isoform-specific shRNAs (shHMGA2-S or shHMGA2-L) following 7 days in culture.

(E) Left: Clonogenic progenitor assay of CD34⁺ CB cells following KD of *HMGA2* isoforms. Cells transduced with shLUC, shHMGA2-S, and shHMGA2-L hairpins were plated 3 days post-infection and CFU potential was measured 14 days post-plating. (right) CFU potential of CD34⁺ CB transduced with hairpins against both *HMGA2* isoforms (shBOTH) was rescued upon overexpression of either the *HMGA2-L* or *HMGA2-S* ORFs.

(F) Phenotypic analysis of the stem cell compartment (CD133⁺CD34⁺CD38⁺) in BM CD34⁺ cells transduced with CTRL, *HMGA2-L*+3'UTRwt, *HMGA2-L*+3'UTRmt, or *HMGA2-S*+3'UTRwt constructs after 7 days in culture.

(G) Clonogenic progenitor assay of CD34⁺ BM cells following overexpression of *HMGA2* isoforms. Cells transduced with CTRL were plated 3 days after infection and CFU potential was measured 14 days post-plating.

Mean ± SEM values are shown for (D)–(G). Analysis of deviance for generalized linear models (CFU analyses) or repeated-measures ANOVA (FACS analyses) were used; **p* < 0.05 or ***p* < 0.01, non-significant (NS).

We first filtered known splicing regulators to 23 candidates (Figure 6A) and then overexpressed each of these factors in PC-3 cells, which endogenously express both *HMGA2* isoforms. Among factors tested, *CLK3* had the strongest effect on *HMGA2* isoform switching (Figure 6B). *CLK3* belongs to the CDC-like kinases (*CLK1–4*) family of dual-specificity protein kinases, which regulate alternative splicing through phosphorylation of serine/arginine-rich domains on direct splicing factors (Colwill et al., 1996). To provide further evidence, we treated PC-3 cells with shRNAs against *CLK3* (shCLK3) and observed a decrease of *HMGA2-S* with a corresponding increase of *HMGA2-L* expression (Figure S5A). Among HSCs profiled, *CLK3* expres-

sion was the highest in CB HSCs (Figure 6C) and correlated with *HMGA2-S* expression across the CB hierarchy (Figure S5B). To investigate whether *CLK3* affects the *HMGA2* splicing pattern in human HSCs, we transduced BM CD34⁺ with lentiviral constructs overexpressing *CLK3* or a CTRL (Figure 6D). BM CD34⁺ cells were chosen for their low endogenous *CLK3* and *HMGA2* levels. RNA-seq analysis 4 days after infection of *CLK3* demonstrated stimulation of expression of *HMGA2-S* (Figures 6E and S5C). Interestingly, expression of an additional isoform bearing a short 3' UTR (*HMGA2-S''*) distinct from *HMGA2-S* and *HMGA2-L* was also stimulated upon *CLK3* O/E; this *HMGA2-S''* isoform is normally expressed at very low levels

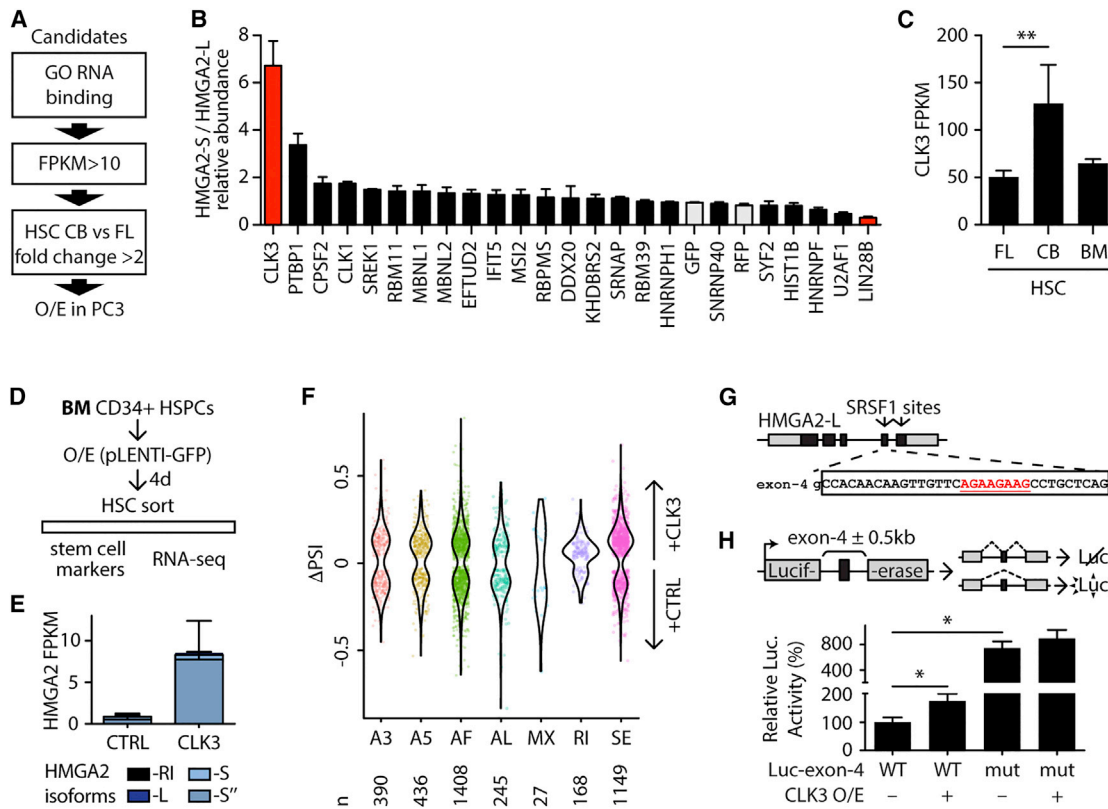


Figure 6. CLK3 Affects HMGA2 Splicing through SRSF1

(A) Schematic representation of the filtering strategy to identify regulators of *HMGA2* splicing. Genes were selected for the GO term “RNA binding” (GO:0003723), minimum expression, and ratio of expression in CB-HSC versus FL-HSC, as in the scheme.

(B) Ratio of expression of *HMGA2-S/HMGA2-L* following overexpression of the indicated candidate splicing factors in PC-3 cells. Controls (GFP and RFP) are shaded in gray. Values were normalized to the *HMGA2-S/HMGA2-L* ratio upon control GFP overexpression and shown as mean \pm SEM.

(C) *CLK3* expression by RNA-seq (in FPKM) in the indicated HSC populations. Mean \pm SD values are shown. FDR < 0.01 (**).

(D) Schematic representation of *CLK3* modulation in BM HSPCs.

(E) *HMGA2* isoform quantification by RNA-seq (in FPKM) in BM-HSCs isolated upon overexpression of *CLK3* or CTRL 4 days post-infection. Mean \pm SD values are shown. PCR validation is shown in Figure S5C.

(F) Violin plot representing distributions of statistically significant ($p < 0.05$) Δ PSI values for different classes of PSI events (as in Figure 1H) in *CLK3* overexpression as compared to vector control. Individual significant events are shown. The number of events of each PSI class are shown below the plot.

(G) Schematic representation of *HMGA2-L* genomic structure (coding exons in black, UTRs in gray). SRSF1 binding motif sites are indicated by arrows in the corresponding exons. Sequence of exon 4 is shown, and the predicted SRSF1 site is underlined in red.

(H) Schematic representation of the luciferase-based splicing reporter constructs. The pcDNA3.1-Luc plasmid contains an intron-spaced Firefly luciferase coding sequence (gray boxes) that produces bioactive luciferase protein only upon proper splicing of the intervening intron. The *HMGA2-L* genomic region encompassing exon 4 (black box) plus 500 bp on either side of the flanking introns (wild-type [WT] or mutated [mut] by deletion of SRSF1 site) was cloned into the intron of pcDNA3.1-Luc. Its inclusion in the luciferase coding sequence abolishes bioactive luciferase. Normalized luciferase activities were tested with or without *CLK3* overexpression and reported with respect to Luc-exon-4 WT set to 100%. Mean \pm SEM values are shown. Repeated-measures ANOVA was used; * $p < 0.05$.

in HSCs (Figures S2A and S2B). A similar effect of stimulating *HMGA2-S* expression was also observed in HPC-5F cells upon *CLK3* O/E (Figure S5D).

To evaluate the impact of *CLK3* O/E on the global repertoire of splicing events in BM-HSCs, we performed a Δ PSI analysis as above (see STAR Methods). For most types of PSI events, approximately the same number of events were induced by *CLK3* O/E as were depleted. However, *CLK3* O/E significantly increased exon skipping (SE) events (Figure 6F, $p = 8.26 \times 10^{-30}$) and promoted intron retention (RI, Figure 6F, $p = 4.99 \times 10^{-8}$). These results suggest a global role of *CLK3* in mediating alternative splicing.

Interestingly, exons preferentially spliced out upon *CLK3* O/E were enriched for SRSF1 binding motifs ($p = 0.0016$) (Park et al., 2016). SRSF1 is known to bind exonic enhancer sequences (ESE) and act as a barrier to prevent exon skipping (Long and Caceres, 2009). As SR proteins are regulated by CLK proteins, we searched for predicted SRSF1 binding sites in *HMGA2*. Motif analyses identified SRSF1 binding motifs only in the *HMGA2-L* mRNA sequence, specifically in exons 4 and 5, which are exclusive to *HMGA2-L* (Figure 6G). To test whether *CLK3*'s effect on *HMGA2* splicing is mediated by SRSF1, we cloned exon 4 of *HMGA2-L* (including flanking intronic regions [500 bp]) into a luciferase splicing reporter

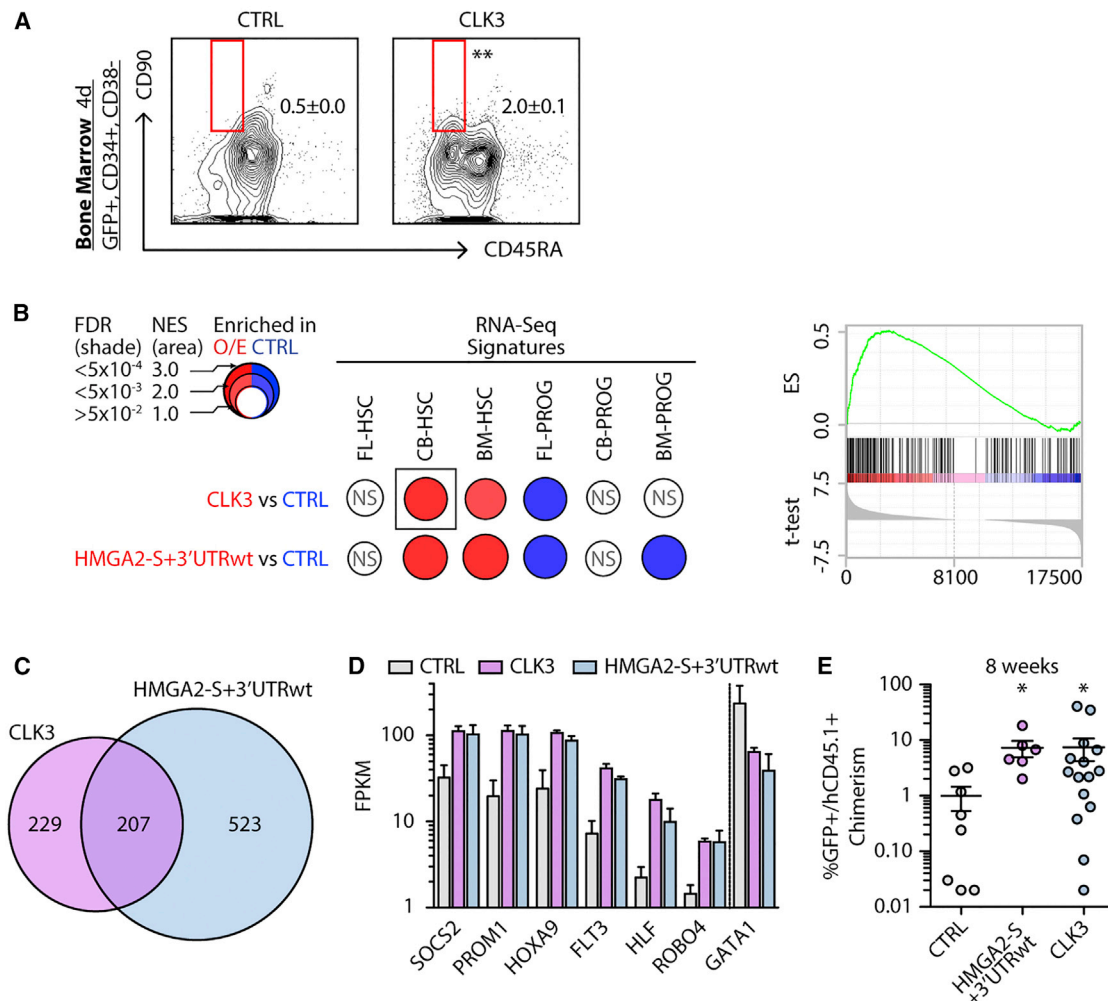


Figure 7. CLK3-HMGA2 Axis Orchestrates an HSC-Specific Program

(A) Phenotypic analysis of HSC content in BM CD34⁺ cells transduced with CTRL or *CLK3* lentiviral constructs 4 days post-infection. Mean \pm SEM values are shown. Unpaired t test was used, ** $p < 0.01$.

(B) BubbleMap visualization (Spinelli et al., 2015) of GSEA results in BM-HSCs upon CTRL, *CLK3*, or *HMGA2-S+3'UTRwt* overexpression. Gene sets were derived from HSC and PROG-specific signatures from Figure 1C (see Table S2C). As indicated in the legend, colors (red versus blue) correspond to the sample label, shades represent statistical significance (FDR), and the area of the circle represents the enrichment (normalized enrichment score, NES). Empty circles correspond to non-significant (NS) enrichments (FDR > 0.05). Representative GSEA plot of the boxed BubbleMap is shown on the right.

(C) Venn diagrams of genes significantly DE (FDR < 0.05) upon *CLK3* or *HMGA2-S+3'UTRwt* overexpression.

(D) RNA-seq-based expression (in FPKM) of representative genes upon CTRL, *CLK3*, and *HMGA2-S+3'UTRwt* overexpression in BM HSCs. Mean \pm SD values are shown. Cufflinks FDR < 0.05 in all comparisons.

(E) Human chimerism as percentage of GFP⁺CD45.1⁺ in the injected femur of xenografted mice 8 weeks after transplantation of BM CD34⁺ HSPCs transduced with lentivirus for *HMGA2-S+3'UTRwt*, *CLK3*, or CTRL. Individual sample, mean \pm SEM values are shown. Mann-Whitney test was used to individually compare each indicated sample with respect to CTRL, * $p < 0.05$.

(Luc-exon-4 WT) (Figure 6H, top) (Martone et al., 2016). A version of *HMGA2-L* exon 4 that is mutated for the SRSF1 binding motif was also generated. Upon *CLK3* O/E, luciferase activity of the WT construct was enhanced, indicating that *CLK3* O/E promotes skipping of the exon containing an SRSF1 binding motif. The observed effect was further enhanced when the SRSF1 site in that exon was mutated (Figure 6H, low). *CLK3* O/E did not further increase luciferase activity of the mutated construct, supporting the direct molecular link between *CLK3* and SRSF1. qPCR in PC-3 cells treated with SRSF1-specific small interfering RNAs (siRNAs) further confirm that depletion of SRSF1 affects

HMGA2 splicing by decreasing *HMGA2-L* and increasing *HMGA2-S* expression (Figure S5E), phenocopying the effect of *CLK3* modulation (Figures 6B and S5A). Collectively, these results indicate that *CLK3* promotes the skipping of *HMGA2-L* exon in a SRSF1-dependent manner.

CLK3-HMGA2-S Axis Orchestrates an HSC-Specific Program

Flow cytometry revealed a >4-fold increase of HSCs upon *CLK3* O/E 4 days post-infection of BM CD34⁺ (as compared to CTRL) (Figure 7A). A similar trend, albeit to a lesser extent, was

observed upon *CLK3* O/E in CD34⁺ CB cells, possibly due to higher endogenous *CLK3* expression (Figure S6A). Next, we evaluated the global effect of *CLK3* O/E on the transcriptional landscape in BM HSCs. GSEA revealed that *CLK3* O/E reinforced a BM-HSC gene signature and reactivated a CB-HSC gene signature (Figure 7B). Interestingly, we observed that *CLK3* O/E reactivates a broad HSC signature in HPC-5F (Figure S6B), similar to the effect observed with forced expression of *HMGA2* ORFs (Figure 3G). Furthermore, the impact of *CLK3* on the HSC transcriptional landscape was phenocopied by *HMGA2*-S+3'UTRwt O/E in BM-HSCs (Figure 7B). On a global level, we detected an overlap of the genes modulated upon *CLK3* and *HMGA2*-S treatment, with ~50% of the total of genes modulated upon *CLK3* O/E displaying the same trend upon *HMGA2*-S O/E (Figure 7C). This included higher expression of key regulators of the HSC program in BM-HSCs transduced with *CLK3* and *HMGA2*-S+3'UTRwt (Figure 7D).

To further support our observation that *CLK3*-mediated promotion of stemness potential is mediated by *HMGA2*-S, we performed a rescue experiment by co-infecting CB CD34⁺ cells with sh*CLK3* and an *HMGA2*-S O/E construct. CFU analysis revealed that sh*CLK3* treatment of CB CD34⁺ significantly reduced E and GEMM colonies (Figure S6C), paralleling the effect of *HMGA2*-S KD (Figure 5E). In contrast, co-overexpression of *HMGA2*-S rescued the output of E and GEMM colonies (Figure S6C).

To evaluate whether elevation of HSC-specific gene expression enhances HSC function *in vivo*, we transduced human BM CD34⁺ cells with *HMGA2*-S+3'UTRwt, *CLK3*, or CTRL vectors and transplanted cells into immunodeficient mice. Human BM CD34⁺ cells display significantly reduced proliferative potential *in vivo* compared to CB and FL cells, corresponding to an age-related decline in HSC function (Bernitz et al., 2016). Consistent with this, CTRL-treated BM cells displayed only ~1% engraftment at 8 weeks post-transplant. In contrast, induction of *HMGA2*-S+3'UTRwt or *CLK3* significantly enhanced the human chimerism (Figure 7E). Collectively, our findings demonstrate that *CLK3*, at least in part by regulating the splicing pattern of *HMGA2*, reinforces an HSC-specific program *in vitro* and *in vivo*.

DISCUSSION

Recent studies have leveraged high-throughput genetic, epigenetic, and transcriptomic data to better understand the underlying mechanisms of hematopoiesis (Notta et al., 2016). Here, we have comprehensively characterized the transcriptional landscape of HSCs along development (FL, CB, and BM), including gene and isoform-level expression of coding genes, as well as expression of non-coding RNAs. Building on prior work (Chen et al., 2014), our analyses highlighted extensive alternative splicing among HSC populations, including a stage-specific alternative splicing pattern for *HMGA2*. Comprehensive functional experiments further reveal that interplay between alternative splicing and miRNA-mediated regulation profoundly impacts regulation and expression of *HMGA2*, with consequences for the molecular identity and behavior of human HSCs.

HMGA2 is an important downstream effector of the LIN28/*let-7* pathway (Viswanathan et al., 2008), and its expression is tightly regulated at its 3' UTR by *let-7* miRNAs (Lee and Dutta, 2007). Expression of aberrant *HMGA2* transcripts is frequently seen in

human malignancies (Schoenmakers et al., 1995) as the result of chromosomal rearrangements, and has been observed in a single patient in a gene therapy trial, as a consequence of insertional mutagenesis that dissociate the *HMGA2* 3' UTR from its protein-coding region (Cavazzana-Calvo et al., 2010). Loss of *let-7* sites has been proposed as the major driver of *HMGA2*-mediated oncogenic transformation (Fedele et al., 1998; Mayr et al., 2007) and promotion of hematopoietic cell proliferation (Ikeda et al., 2011). Here, we report that CB-HSCs express an alternative *HMGA2* isoform bearing a 3' UTR devoid of miRNA sites (*HMGA2*-S) and that expression of *HMGA2*-S allows for preserved expression and function of *HMGA2* in spite of physiologically high levels of *let-7* and other miRNAs present in CB-HSCs. Independent reports have implicated *HMGA2* in promoting cell proliferation and stem cell properties in different contexts (Copley et al., 2013; Ikeda et al., 2011; Li et al., 2007; Nishino et al., 2008). Our work expands the role of *HMGA2* in HSCs and provides evidence for similar functions of the proteins encoded by the two *HMGA2* isoforms.

Our work also delineated the molecular mechanism for differential *HMGA2* splicing observed across HSCs. Here, we describe the role of a splicing kinase, *CLK3*, in impacting HSC development by promoting expression of an *HMGA2* isoform insensitive to miRNA-mediated targeting. Indeed, we observed a substantial overlap between genes modulated by either *CLK3* or *HMGA2*-S. We also demonstrate that enforced expression of *CLK3* and *HMGA2*-S can induce a more proliferative phenotype in BM-HSCs by reactivating a CB-specific transcriptional signature and promoting engraftment of human BM HSPCs, which normally display low repopulating capacity.

Furthermore, we demonstrated that *CLK3* stimulates exon skipping, including at *HMGA2*. A dynamic cycle of phosphorylation and dephosphorylation of SR proteins is essential for splicing (Mermoud et al., 1994). Among splicing kinases, CLK proteins have broad roles in this phosphorylation process to regulate SR proteins (Ngo et al., 2005; Aubol et al., 2016). In line with previous observations that high levels of CLK inhibit the activity of SR proteins in promoting splicing (Prasad et al., 1999), we show that (1) exons preferentially spliced out upon *CLK3* O/E are enriched for SRSF1 binding sites; (2) only *HMGA2*-L (and not *HMGA2*-S) contains SRSF1 binding sites; and (3) *CLK3* O/E affects *HMGA2*-L proper splicing by preventing SRSF1 activity at its binding sites. Thus, in the context of *HMGA2*, we have demonstrated that *CLK3* acts through SRSF1 to shift the balance of *HMGA2*-L versus *HMGA2*-S splicing.

In summary, we show marked differences among HSC populations at different developmental stages and implicate alternative splicing as a mechanism that contributes to the transcriptional diversity. Our comprehensive map of the transcriptome of HSCs represents a valuable tool for understanding the mechanisms of hematopoiesis that can be applied to complement and improve cell fate conversion and HSC expansion approaches.

Our work also expands the canonical LIN28/*let-7* pathway, where LIN28 proteins inhibit *let-7* biogenesis, which in turn repress expression of target genes, including *HMGA2* (Lee and Dutta, 2007). Our results highlight a physiologic isoform of *HMGA2* that escapes regulation by the upstream LIN28/*let-7* pathway. *CLK3* appears to function as a tuner that, by regulating the balance of *HMGA2* isoforms, impacts the developmental identity of HSCs. Collectively, our findings open up new

directions of investigation into the mechanisms of altered *HMGA2* splicing that might contribute to developmental regulation and malignancies.

STAR★METHODS

Detailed methods are provided in the online version of this paper and include the following:

- **KEY RESOURCES TABLE**
- **CONTACT FOR REAGENTS AND RESOURCE SHARING**
- **EXPERIMENTAL MODEL AND SUBJECT DETAILS**
 - Primary hematopoietic cell source and FACS analyses
 - Cell culture and viral transduction
 - Colony forming unit assays
 - Mouse transplantation and assessment of human cell engraftment
 - Luciferase reporter assays
 - Transfection of miRNA hairpin inhibitors
- **METHOD DETAILS**
 - RNA and DNA sequencing libraries
 - miRNA profiling and analysis
 - RNA-seq alignment and transcript assembly
 - Differential expression analyses, RT-PCR and qPCR
 - Definition of HSC transcriptional signatures
 - Gene set enrichment analysis (GSEA)
 - ChIP-Seq alignment and promoter analysis
 - let-7 target analysis
 - PSI analysis
 - Splicing factor screen
 - Identification of SRSF1 binding motif
 - RNA binding protein enrichment
- **QUANTIFICATION AND STATISTICAL ANALYSIS**
- **DATA AND SOFTWARE AVAILABILITY**

SUPPLEMENTAL INFORMATION

Supplemental Information includes six figures and four tables and can be found with this article online at <https://doi.org/10.1016/j.stem.2018.03.012>.

ACKNOWLEDGMENTS

We are grateful to Trista North for critical review of the manuscript; Tarjei Mikelsen, Michael Ziller, and Areum Han for technical assistance and for helpful discussion; Ronald Mathieu and Mahnaz Paktinat at the BCH Flow Cytometry core for sorting; Annamaria Carissimo for assistance with statistical analyses; and Julie Martone and Irene Bozzoni for providing the plasmid for the splicing assay. This work is supported by grants to G.Q.D. from the NIH NIDDK (R24-DK092760 and U54-DK110805) and the NHLBI Progenitor Cell Biology Consortium (U01-HL100001). G.Q.D. was also supported by the Howard Hughes Medical Institute and is an affiliate of the Broad Institute. Additional support was given to J.N.H. from NIH grant R01DK075787; to A.M. from New York Stem Cell Foundation; to A.C. from NCI Outstanding Investigator Award (R35 CA197745); to A.C., B.S., and F.M.G. from Centers for Cancer Systems Biology (U54 CA209997); and to D.C. from Fondazione Telethon Core Grant. D.C. is an Armenise-Harvard Foundation Career Development Award Investigator and a Rita-Levi Montalcini Program Fellow from MIUR. A.M. is a New York Stem Cell Foundation Robertson Investigator. M.C. was supported by EMBO Long Term Fellowship and Leukemia and Lymphoma Society Fellowship. L.T.V. was supported by the NSF Graduate Research Fellowship. K.M.T. was supported by the HHMI International Student Research Fellowship and the Herchel Smith Graduate Fellowship.

AUTHOR CONTRIBUTIONS

M.C. and G.Q.D. conceived the experimental plan. M.C., M.H.G., and D.C. wrote the manuscript. M.C., L.W., B.T.-V., D.C., K.M.T., J.B., and A.B. performed experimental work. S.D., L.T.V., and L.W. performed intra-femoral injections and provided HPC-5F cells. P.M.S. assisted with mouse work. M.H.G., C.T., K.C., and P.C. processed and analyzed data. B.S. and F.M.G. performed gene network analyses. D.C. supervised computational analyses. G.Q.D., J.N.H., A.M., J.L.R., and A.C. provided mentoring and assisted with data interpretation.

DECLARATION OF INTERESTS

G.Q.D. holds equity interest in True North Therapeutics and 28/7 Therapeutics.

Received: January 26, 2017

Revised: October 10, 2017

Accepted: March 14, 2018

Published: April 5, 2018

REFERENCES

- Agarwal, V., Bell, G.W., Nam, J.-W., and Bartel, D.P. (2015). Predicting effective microRNA target sites in mammalian mRNAs. *eLife* 4.
- Alamancos, G.P., Pagès, A., Trincado, J.L., Bellora, N., and Eyras, E. (2015). Leveraging transcript quantification for fast computation of alternative splicing profiles. *RNA* 21, 1521–1531.
- Aubol, B.E., Wu, G., Keshwani, M.M., Movassat, M., Fattet, L., Hertel, K.J., Fu, X.-D., and Adams, J.A. (2016). Release of SR proteins from CLK1 by SRPK1: A symbiotic kinase system for phosphorylation control of pre-mRNA splicing. *Mol. Cell* 63, 218–228.
- Babovic, S., and Eaves, C.J. (2014). Hierarchical organization of fetal and adult hematopoietic stem cells. *Exp. Cell Res.* 329, 185–191.
- Bernitz, J.M., Kim, H.S., MacArthur, B., Sieburg, H., and Moore, K. (2016). Hematopoietic stem cells count and remember self-renewal divisions. *Cell* 167, 1296–1309.
- Cabezas-Wallscheid, N., Klimmeck, D., Hansson, J., Lipka, D.B., Reyes, A., Wang, Q., Weichenhan, D., Lier, A., von Paleske, L., Renders, S., et al. (2014). Identification of regulatory networks in HSCs and their immediate progeny via integrated proteome, transcriptome, and DNA methylome analysis. *Cell Stem Cell* 15, 507–522.
- Cabilii, M.N., Trapnell, C., Goff, L., Koziol, M., Tazon-Vega, B., Regev, A., and Rinn, J.L. (2011). Integrative annotation of human large intergenic noncoding RNAs reveals global properties and specific subclasses. *Genes Dev.* 25, 1915–1927.
- Cacchiarelli, D., Trapnell, C., Ziller, M.J., Soumillon, M., Cesana, M., Karnik, R., Donaghey, J., Smith, Z.D., Ratanasirintrawoot, S., Zhang, X., et al. (2015). Integrative analyses of human reprogramming reveal dynamic nature of induced pluripotency. *Cell* 162, 412–424.
- Cavazzana-Calvo, M., Payen, E., Negre, O., Wang, G., Hehir, K., Fusil, F., Down, J., Denaro, M., Brady, T., Westerman, K., et al. (2010). Transfusion independence and *HMGA2* activation after gene therapy of human β -thalassaemia. *Nature* 467, 318–322.
- Chadwick, K., Wang, L., Li, L., Menendez, P., Murdoch, B., Rouleau, A., and Bhatia, M. (2003). Cytokines and BMP-4 promote hematopoietic differentiation of human embryonic stem cells. *Blood* 102, 906–915.
- Chambers, J.M., and Hastie, T.J. (1991). *Statistical Models in S* (Pacific Grove, CA: Wadsworth & Brooks/Cole).
- Chen, L., Kostadima, M., Martens, J.H.A., Canu, G., Garcia, S.P., Turro, E., Downes, K., Macaulay, I.C., Bielczyk-Maczynska, E., Coe, S., et al. (2014). Transcriptional diversity during lineage commitment of human blood progenitors. *Science* 345, 1251033.
- Colombo, D.F., Burger, L., Baubec, T., and Schübeler, D. (2017). Binding of high mobility group A proteins to the mammalian genome occurs as a function of AT-content. *PLoS Genet.* 13, e1007102.

- Colwill, K., Pawson, T., Andrews, B., Prasad, J., Manley, J.L., Bell, J.C., and Duncan, P.I. (1996). The Clk/Sty protein kinase phosphorylates SR splicing factors and regulates their intranuclear distribution. *EMBO J.* *15*, 265–275.
- Copley, M.R., Babovic, S., Benz, C., Knapp, D.J., Beer, P.A., Kent, D.G., Wohrer, S., Treloar, D.Q., Day, C., Rowe, K., et al. (2013). The Lin28b-let-7-Hmga2 axis determines the higher self-renewal potential of fetal haematopoietic stem cells. *Nat. Cell Biol.* *15*, 916–925.
- Crews, L.A., Balaian, L., Delos Santos, N.P., Leu, H.S., Court, A.C., Lazzari, E., Sadarangani, A., Zipeto, M.A., La Clair, J.J., Villa, R., et al. (2016). RNA splicing modulation selectively impairs leukemia stem cell maintenance in secondary human AML. *Cell Stem Cell* *19*, 599–612.
- Doulatov, S., Notta, F., Laurenti, E., and Dick, J.E. (2012). Hematopoiesis: A human perspective. *Cell Stem Cell* *10*, 120–136.
- Doulatov, S., Vo, L.T., Chou, S.S., Kim, P.G., Arora, N., Li, H., Hadland, B.K., Bernstein, I.D., Collins, J.J., Zon, L.I., and Daley, G.Q. (2013). Induction of multipotential hematopoietic progenitors from human pluripotent stem cells via respecification of lineage-restricted precursors. *Cell Stem Cell* *13*, 459–470.
- Ebina, W., and Rossi, D.J. (2015). Transcription factor-mediated reprogramming toward hematopoietic stem cells. *EMBO J.* *34*, 694–709.
- Fatica, A., and Bozzoni, I. (2014). Long non-coding RNAs: New players in cell differentiation and development. *Nat. Rev. Genet.* *15*, 7–21.
- Fedele, M., Berlingieri, M.T., Scala, S., Chiariotti, L., Viglietto, G., Rippel, V., Bullerdiek, J., Santoro, M., and Fusco, A. (1998). Truncated and chimeric HMGI-C genes induce neoplastic transformation of NIH3T3 murine fibroblasts. *Oncogene* *17*, 413–418.
- Han, J., Pedersen, J.S., Kwon, S.C., Belair, C.D., Kim, Y.-K., Yeom, K.-H., Yang, W.-Y., Haussler, D., Blelloch, R., and Kim, V.N. (2009). Posttranscriptional crossregulation between Drosha and DGCR8. *Cell* *136*, 75–84.
- Harrow, J., Frankish, A., Gonzalez, J.M., Tapanari, E., Diekhans, M., Kokocinski, F., Aken, B.L., Barrell, D., Zadissa, A., Searle, S., et al. (2012). GENCODE: the reference human genome annotation for The ENCODE Project. *Genome Res* *22*, 1760–1774.
- Heinz, S., Benner, C., Spann, N., Bertolino, E., Lin, Y.C., Laslo, P., Cheng, J.X., Murre, C., Singh, H., and Glass, C.K. (2010). Simple combinations of lineage-determining transcription factors prime cis-regulatory elements required for macrophage and B cell identities. *Mol. Cell* *38*, 576–589.
- Ikeda, K., Mason, P.J., and Bessler, M. (2011). 3'UTR-truncated Hmga2 cDNA causes MPN-like hematopoiesis by conferring a clonal growth advantage at the level of HSC in mice. *Blood* *117*, 5860–5869.
- Kazmierczak, B., Rosigkeit, J., Wanschura, S., Meyer-Bolte, K., Van de Ven, W.J., Kayser, K., Kriehoff, B., Kastendiek, H., Bartnitzke, S., and Bullerdiek, J. (1996). HMGI-C rearrangements as the molecular basis for the majority of pulmonary chondroid hamartomas: A survey of 30 tumors. *Oncogene* *12*, 515–521.
- Langmead, B., and Salzberg, S.L. (2012). Fast gapped-read alignment with Bowtie 2. *Nat. Methods* *9*, 357–359.
- Lee, Y.S., and Dutta, A. (2007). The tumor suppressor microRNA let-7 represses the HMGA2 oncogene. *Genes Dev.* *21*, 1025–1030.
- Li, O., Li, J., and Dröge, P. (2007). DNA architectural factor and proto-oncogene HMGA2 regulates key developmental genes in pluripotent human embryonic stem cells. *FEBS Lett.* *581*, 3533–3537.
- Long, J.C., and Caceres, J.F. (2009). The SR protein family of splicing factors: Master regulators of gene expression. *Biochem. J.* *417*, 15–27.
- Martone, J., Briganti, F., Legnini, I., Morlando, M., Picillo, E., Sthandier, O., Politano, L., and Bozzoni, I. (2016). The lack of the Celf2a splicing factor converts a Duchenne genotype into a Becker phenotype. *Nat. Commun.* *7*, 10488.
- Mayr, C., Hemann, M.T., and Bartel, D.P. (2007). Disrupting the pairing between let-7 and Hmga2 enhances oncogenic transformation. *Science* *315*, 1576–1579.
- McKinney-Freeman, S., Cahan, P., Li, H., Lacadie, S.A., Huang, H.-T., Curran, M., Loewer, S., Naveiras, O., Kathrein, K.L., Konantz, M., et al. (2012). The transcriptional landscape of hematopoietic stem cell ontogeny. *Cell Stem Cell* *11*, 701–714.
- Mermoud, J.E., Cohen, P.T., and Lamond, A.I. (1994). Regulation of mammalian spliceosome assembly by a protein phosphorylation mechanism. *EMBO J.* *13*, 5679–5688.
- Mikkola, H.K.A., and Orkin, S.H. (2006). The journey of developing hematopoietic stem cells. *Development* *133*, 3733–3744.
- Miraglia, S., Godfrey, W., Yin, A.H., Atkins, K., Warnke, R., Holden, J.T., Bray, R.A., Waller, E.K., and Buck, D.W. (1997). A novel five-transmembrane hematopoietic stem cell antigen: Isolation, characterization, and molecular cloning. *Blood* *90*, 5013–5021.
- Ngo, J.C.K., Chakrabarti, S., Ding, J.-H., Velazquez-Dones, A., Nolen, B., Aubol, B.E., Adams, J.A., Fu, X.-D., and Ghosh, G. (2005). Interplay between SRPK and Clk/Sty kinases in phosphorylation of the splicing factor ASF/SF2 is regulated by a docking motif in ASF/SF2. *Mol. Cell* *20*, 77–89.
- Nishino, J., Kim, I., Chada, K., and Morrison, S.J. (2008). Hmga2 promotes neural stem cell self-renewal in young but not old mice by reducing p16Ink4a and p19Arf Expression. *Cell* *135*, 227–239.
- Notta, F., Zandi, S., Takayama, N., Dobson, S., Gan, O.I., Wilson, G., Kaufmann, K.B., McLeod, J., Laurenti, E., Dunant, C.F., et al. (2016). Distinct routes of lineage development reshape the human blood hierarchy across ontogeny. *Science* *351*, aab2116.
- Novershtern, N., Subramanian, A., Lawton, L.N., Mak, R.H., Haining, W.N., McConkey, M.E., Habib, N., Yosef, N., Chang, C.Y., Shay, T., et al. (2011). Densely interconnected transcriptional circuits control cell states in human hematopoiesis. *Cell* *144*, 296–309.
- Ozturk, N., Singh, I., Mehta, A., Braun, T., and Barreto, G. (2014). HMGA proteins as modulators of chromatin structure during transcriptional activation. *Front. Cell Dev. Biol.* *2*, 5.
- Park, J.W., Jung, S., Rouchka, E.C., Tseng, Y.-T., and Xing, Y. (2016). rMAPS: RNA map analysis and plotting server for alternative exon regulation. *Nucleic Acids Res.* *44* (W1), W333–W338.
- Prasad, J., Colwill, K., Pawson, T., and Manley, J.L. (1999). The protein kinase Clk/Sty directly modulates SR protein activity: Both hyper- and hypophosphorylation inhibit splicing. *Mol. Cell Biol.* *19*, 6991–7000.
- Qian, P., He, X.C., Paulson, A., Li, Z., Tao, F., Perry, J.M., Guo, F., Zhao, M., Zhi, L., Venkatraman, A., et al. (2016). The Dlk1-Gtl2 locus preserves LT-HSC function by inhibiting the PI3K-mTOR pathway to restrict mitochondrial metabolism. *Cell Stem Cell* *18*, 214–228.
- Quinlan, A.R., and Hall, I.M. (2010). BEDTools: A flexible suite of utilities for comparing genomic features. *Bioinformatics* *26*, 841–842.
- Rentas, S., Holzapfel, N., Belew, M.S., Pratt, G., Voisin, V., Wilhelm, B.T., Bader, G.D., Yeo, G.W., and Hope, K.J. (2016). Musashi-2 attenuates AHR signaling to expand human haematopoietic stem cells. *Nature* *532*, 508–511.
- Robinson, J.T., Thorvaldsdóttir, H., Winckler, W., Guttman, M., Lander, E.S., Getz, G., and Mesirov, J.P. (2011). Integrative genomics viewer. *Nat. Biotechnol.* *29*, 24–26.
- Schoenmakers, E.F., Wanschura, S., Mols, R., Bullerdiek, J., Van den Berghe, H., and Van de Ven, W.J. (1995). Recurrent rearrangements in the high mobility group protein gene, HMGI-C, in benign mesenchymal tumours. *Nat. Genet.* *10*, 436–444.
- Shyh-Chang, N., and Daley, G.Q. (2013). Lin28: Primal regulator of growth and metabolism in stem cells. *Cell Stem Cell* *12*, 395–406.
- Sperling, A.S., Gibson, C.J., and Ebert, B.L. (2017). The genetics of myelodysplastic syndrome: From clonal haematopoiesis to secondary leukaemia. *Nat. Rev. Cancer* *17*, 5–19.
- Spinelli, L., Carpentier, S., Montañana Sanchis, F., Dalod, M., and Vu Manh, T.-P. (2015). BubbleGUM: Automatic extraction of phenotype molecular signatures and comprehensive visualization of multiple Gene Set Enrichment Analyses. *BMC Genomics* *16*, 814.
- Stunnenberg, H.G., and Hirst, M.; International Human Epigenome Consortium (2016). The International Human Epigenome Consortium: A blueprint for scientific collaboration and discovery. *Cell* *167*, 1897.

- Subramanian, A., Tamayo, P., Mootha, V.K., Mukherjee, S., Ebert, B.L., Gillette, M.A., Paulovich, A., Pomeroy, S.L., Golub, T.R., Lander, E.S., and Mesirov, J.P. (2005). Gene set enrichment analysis: A knowledge-based approach for interpreting genome-wide expression profiles. *Proc. Natl. Acad. Sci. USA* *102*, 15545–15550.
- Trapnell, C., Roberts, A., Goff, L., Pertea, G., Kim, D., Kelley, D.R., Pimentel, H., Salzberg, S.L., Rinn, J.L., and Pachter, L. (2012). Differential gene and transcript expression analysis of RNA-seq experiments with TopHat and Cufflinks. *Nat. Protoc.* *7*, 562–578.
- Uhlén, M., Fagerberg, L., Hallström, B.M., Lindskog, C., Oksvold, P., Mardinoglu, A., Sivertsson, Å., Kampf, C., Sjöstedt, E., Asplund, A., et al. (2015). Proteomics. Tissue-based map of the human proteome. *Science* *347*, 1260419.
- Vedi, A., Santoro, A., Dunant, C.F., Dick, J.E., and Laurenti, E. (2016). Molecular landscapes of human hematopoietic stem cells in health and leukemia. *Ann. N Y Acad. Sci.* *1370*, 5–14.
- Viswanathan, S.R., Daley, G.Q., and Gregory, R.I. (2008). Selective blockade of microRNA processing by Lin28. *Science* *320*, 97–100.
- Wang, E.T., Sandberg, R., Luo, S., Khrebtkova, I., Zhang, L., Mayr, C., Kingsmore, S.F., Schroth, G.P., and Burge, C.B. (2008). Alternative isoform regulation in human tissue transcriptomes. *Nature* *456*, 470–476.
- Wang, X., Juan, L., Lv, J., Wang, K., Sanford, J.R., and Liu, Y. (2011). Predicting sequence and structural specificities of RNA binding regions recognized by splicing factor SRSF1. *BMC Genomics* *12* (Suppl 5), S8.
- Winter, N., Nimzyk, R., Börsche, C., Meyer, A., and Bullerdiek, J. (2011). Chromatin immunoprecipitation to analyze DNA binding sites of HMGA2. *PLoS ONE* *6*, e18837.
- Wong, J.J.-L., Ritchie, W., Ebner, O.A., Selbach, M., Wong, J.W.H., Huang, Y., Gao, D., Pinello, N., Gonzalez, M., Baidya, K., et al. (2013). Orchestrated intron retention regulates normal granulocyte differentiation. *Cell* *154*, 583–595.
- Yoshida, K., Sanada, M., Shiraishi, Y., Nowak, D., Nagata, Y., Yamamoto, R., Sato, Y., Sato-Otsubo, A., Kon, A., Nagasaki, M., et al. (2011). Frequent pathway mutations of splicing machinery in myelodysplasia. *Nature* *478*, 64–69.

STAR★METHODS

KEY RESOURCES TABLE

REAGENT or RESOURCE	SOURCE	IDENTIFIER
Antibodies		
CD34 PE-Cy7	BD Biosciences	Cat. 348791; CLONE 8G12
CD38 PE-Cy5	BD Biosciences	Cat. 555461; CLONE HIT2
CD90 PE	BD Biosciences	Cat. 555596; CLONE 5E10
CD45RA FITC	BioLegend	Cat. 304105; CLONE HI100
DAPI solution	BD Biosciences	Cat. 564907
CD45RA V450	BD Biosciences	Cat. 560362; CLONE HI100
CD133/1 APC	Miltenyi Biotec	Cat. 130-090-826; CLONE AC133
CD19 PE	BD Biosciences	Cat. 349209; CLONE 4G7
CD45 PE-Cy5	Coulter	CLONE Immu19.2
CD33 APC	BD Biosciences	Cat. 340474; CLONE P67.6
CD45 APC-Cy7	BD Biosciences	Cat. 561863; CLONE 2D1
V5	MBL	Cat. M167-3
H3K4me2	Diagenode	Cat. 035-050
Biological Samples		
Cord Blood CD34+ Cells	Lonza	Cat. 2C-101
Cord Blood CD34+ Cells	AllCells	Cat. CB008F
Fetal Liver CD34+ Cells	AllCells	Cat. FL-CD34-002F
Bone Marrow CD34+ Cells	AllCells	Cat. ABM017F
Bone Marrow CD34+ Cells	Lonza	Cat. 2M-101C
Chemicals, Peptides, and Recombinant Proteins		
Actinomycin D	Sigma-Aldrich	Cat. A1410
Doxycycline Hyclate	Sigma-Aldrich	Cat. D9891
Protamine Sulfate	Sigma-Aldrich	Cat. P4020
Recombinant Human SCF	Peprotech	Cat. 300-07
Recombinant Human FLT3L	Peprotech	Cat. 300-19
Recombinant Human TPO	Peprotech	Cat. 300-18
Recombinant Human IL6	Peprotech	Cat. 200-06
Retronectin	Clontech	Cat. T100A
DOTAP Liposomal Transfection Reagent	Sigma-Aldrich	Cat. 11202375001
DharmaFECT Duo Transfection Reagent	Dharmacon	Cat. T-2010-03
Critical Commercial Assays		
Dual-Luciferase Reporter Assay System	Promega	Cat. E1910
TruSeq RNA Library Prep Kit v2	Illumina	Cat. RS-122-2001
SMART-Seq v4 Ultra Low Input RNA Kit	Clontech	Cat. 634888
Nextera XT DNA Library Preparation Kit	Illumina	Cat. FC-131-1024
nCounter Human v2 miRNA Expression Assay	NanoString Technologies	Cat. GXA-MIR2-24
ChIP-Seq Assay	Broad Institute Epigenomics Program	N/A
Experimental Models: Cell Lines		
PC-3	ATCC	Cat. CRL-1435
K562	ATCC	Cat. CCL-243
HPC and HPC-5F	Doulatov et al., 2013	N/A
DGCR8 knockout MEF	Novus Biologicals	Cat. NBP2-25171

(Continued on next page)

Continued

REAGENT or RESOURCE	SOURCE	IDENTIFIER
Experimental Models: Organisms/Strains		
NOD/LtSz-scidIL2Rnull (NSG)	Jackson Laboratory	N/A
Deposited Data		
RNA-seq, ChIP-seq, miRNA nanostring data	In this paper	GEO: GSE109093
TargetScan	Agarwal et al., 2015	v7
MSigDb	Subramanian et al., 2005	v6.1
Blueprint Epigenome dataset	Stunnenberg et al., 2016	7th data release
Gencode gene annotations	Harrow et al., 2012	v17, v19
Human reference genome, hg19	UCSC Genome Browser	hg19
SRSF1 motifs	Wang et al., 2011	N/A
Oligonucleotides		
HMGA2-common_FW	AGCGCCTCAGAAGAGAGGAC	N/A
HMGA2-L_RV	TGAGGATGTCTCTTCAGTTTCC	N/A
HMGA2-S_RV	TGGAAGAAAGGCTTCTAAGCTG	N/A
HMGA2-RI_RV	AGGCTCCTGTAGTCAGTCATTG	N/A
HMGA2-S''_RV	TGAAGACACTTTCCTTGGATCC	N/A
HMGA2-L-ORF_FW	AGACCTAGGAAATGGCCACA	N/A
HMGA2-L-ORF_RV	GTCCTCTTCGGCAGACTCTT	N/A
HMGA2-S-ORF_FW	AGTCCCTCTAAAGCAGCTCA	N/A
HMGA2-S-ORF_RV	TGAACACCACATGACACCAA	N/A
HMGA2-ex2-ORF_FW	GAACCAACCGGTGAGCCCT	N/A
HMGA2-ex2-ORF_RV	CTTTTGAGCTGCTTTAGAGGG	N/A
PROM1_FW	CAGAAGGCATATGAATCCAAAA	N/A
PROM1_RV	GGTGCATTTCTCCACCACAT	N/A
QuantiTect Primer Assay Hs_CLK3_1_SG	QIAGEN	Cat. QT00197428 Prod. 249900
QuantiTect Primer Assay Hs_SRSF1_1_SG	QIAGEN	Cat. QT00203056 Prod. 249900
QuantiTect Primer Assay Hs_HPRT1_1_SG	QIAGEN	Cat. QT00059066 Prod. 249900
miScript Primer Assay (miRNAs in this paper)	QIAGEN	Cat. MS000XXXXX Prod. 218300
miScript Primer Assay Hs_RNU6-2_11	QIAGEN	Cat. MS00033740 Prod.218300
ON-TARGETplus Human SRSF1 (6426) siRNA pool	Dharmacon	Cat. L-018672-01-0005
ON-TARGETplus Non-targeting pool	Dharmacon	Cat. D-001810-10-05
miRIDIAN Hairpin Inhibitor (miRNAs in this paper)	Dharmacon	Cat. IH-HMR-XX-0002
miRIDIAN Hairpin Inhibitor Negative Control #1	Dharmacon	Cat. IN-001005-01-05
miRIDIAN Hairpin Inhibitor Negative Control #2	Dharmacon	Cat. IN-002005-01-05
miRIDIAN Mimic (miRNAs in this paper)	Dharmacon	Cat. C-HMR-XX-0002
miRIDIAN Mimic Negative Control #1	Dharmacon	Cat. CN-001000-01-05
Recombinant DNA		
pLVX_HMGA2-L_ORF_V5_PURO	In this paper	N/A
pLVX_HMGA2-S_ORF_V5_PURO	In this paper	N/A
pLVX_CTRL_V5_PURO	In this paper	N/A
pSMAL_HMGA2-L_ORF_BFP (RNAi resistant)	In this paper	N/A
pSMAL_HMGA2-S_ORF_BFP (RNAi resistant)	In this paper	N/A
pSMAL_CTRL_BFP	In this paper	N/A
pSMAL_HMGA2-L_GFP	In this paper	N/A
pSMAL_HMGA2-S_GFP	In this paper	N/A
pSMAL_HMGA2-L+3'UTRwt_GFP	In this paper	N/A
pSMAL_HMGA2-L+3'UTRmt_GFP	In this paper	N/A
pSMAL_HMGA2-S+3'UTRwt_GFP	In this paper	N/A

(Continued on next page)

Continued

REAGENT or RESOURCE	SOURCE	IDENTIFIER
pSMAL_CLK3_GFP	In this paper	N/A
pSMAL_CTRL_GFP	In this paper	N/A
pLKO.1_shRNA_HMGA2-L_1	In this paper	N/A
pLKO.1_shRNA_HMGA2-L_2	In this paper	N/A
pLKO.1_shRNA_HMGA2-S_1	In this paper	N/A
pLKO.1_shRNA_HMGA2-S_2	In this paper	N/A
pLKO.1_shRNA_BOTH	In this paper	N/A
pLKO.1_shRNA_CLK3_1	Sigma-Aldrich	TRCN0000196926
pLKO.1_shRNA_CLK3_2	Sigma-Aldrich	TRCN0000000749
pLKO.1_shRNA_LUC	In this paper	N/A
pLX_TRC304/317_splicing_regulators_ORFs	Broad Institute GPP	N/A
psiCHECK2_Rluc-3'UTRwt_HMGA2-L	In this paper	N/A
psiCHECK2_Rluc-3'UTRmt_HMGA2-L	In this paper	N/A
psiCHECK2_Rluc-3'UTRwt_HMGA2-S	In this paper	N/A
pcDNA3.1_Luc-exon-4-WT (HMGA2-L)	In this paper	N/A
pcDNA3.1_Luc-exon-4-mut (HMGA2-L)	In this paper	N/A
Software and Algorithms		
BEDTools	Quinlan and Hall, 2010	v2.2.6
Cufflinks	Trapnell et al., 2012	v2.2.1
TopHat	Trapnell et al., 2012	v2.0.14
cummeRbund	Trapnell et al., 2012	v2.20.0
Bowtie2	Langmead and Salzberg, 2012	v2.2.1
GSEA	Subramanian et al., 2005	v2.0
BubbleGUM	Spinelli et al., 2015	v1.3.19
IGV	Robinson et al., 2011	v2.3
SUPPA	Alamancos et al., 2015	v2.2.1
rMAPS	Park et al., 2016	v1.0.6
HOMER	Heinz et al., 2010.	v4.9
R	The R Project	v3.1
Python	Python	v2.7

CONTACT FOR REAGENTS AND RESOURCE SHARING

Further information and requests for resources and reagents should be directed to and will be fulfilled by the Lead Contact, George Q. Daley (George.Daley@childrens.harvard.edu)

EXPERIMENTAL MODEL AND SUBJECT DETAILS**Primary hematopoietic cell source and FACS analyses**

Human CD34⁺ cells (Lonza and AllCells) from all sources were obtained as viable frozen states. The ages of the individuals used for the profiling and treatments are as follows: FL-CD34⁺ (17-20 weeks of gestation); CB-CD34⁺ (newborns); BM-CD34⁺ (24-36 years old). For the generation of HSC/PROG transcriptional profiles, at least three distinct lot numbers, each corresponding to independent individuals or pools of distinct individuals (of random male or female samples), were utilized to attain maximal representation. For each biological replicate, HSC and PROG populations were sorted from the same pool of cells. Cells were stained and sorted using a BD FACS Aria II cell sorter for panels of cell surface markers and dyes as indicated below.

HSC panel: CD34 PE-Cy7 (8G12; BD), CD38 PE-Cy5 (HIT2; BD), CD90 PE (5E10; BD), CD45RA-FITC (HI100; BioLegend), DAPI
 PROG panel: CD34 PE-Cy7 (8G12; BD), CD38 PE-Cy5 (HIT2; BD), DAPI
 Stem Cell panel: CD34 PE-Cy7 (8G12; BD), CD38 PE-Cy5 (HIT2; BD), CD90 PE (5E10; BD), CD45RA-V450 (HI100; BD), CD133/1-APC (AC133; Miltenyi Biotec)

Cell culture and viral transduction

All cell culture incubations were performed at 37°C with 5% CO₂. cDNA sequences for overexpression were cloned into a pSMAL-GFP or pSMAL-BFP (Doulatov et al., 2013) or pLVX-PURO (Clontech) lentiviral backbone, using Infusion HD Cloning Kit (Clontech). HMGA2 cDNAs were cloned as full ORF sequences including wild-type or mutated 3'UTRs (see below), as ORFs only, or as RNAi-resistant ORFs (by degenerating the shRNA target sequences). For RNA interference, shRNA sequences were cloned in the pLKO.1_hPGK-Puro-CMV-tGFP lentiviral backbone (Sigma-Aldrich). Lentiviral particle productions and quantifications were performed using standard procedures. CB and BM CD34⁺ cells were thawed and plated in X-VIVO media (Lonza) supplemented with 20% BIT 9500 (StemCell Technologies), 2 mM L-glutamine, and 100 U/ml penicillin/streptomycin, and incubated for 4-6 hours before transduction. Cells were then seeded on retronectin-coated (10 µg/cm²) 96 well plates (Clontech) at a density of 0.5-1x10⁵ cells per well, and viral particles were added at a multiplicity of infection (MOI) of 30-50 (for the KD treatments) or 100 (for the overexpression treatments) in a final volume of 150 µl. The following cytokines were used along with protamine sulfate at 8 µg/ml (Sigma-Aldrich): stem cell factor (SCF) 100 ng/ml, Flt3 ligand (FLT3-L) 100 ng/ml, thrombopoietin (TPO) 50 ng/ml, and interleukin 6 (IL-6) 20 ng/ml (all PeproTech). Cells were then spininfected for 1 hr at 2500 rpm at room temperature (RT) and subsequently incubated for a minimum of 24 hr before changing media. Cells were then expanded in StemSpan SFEM (StemCell Technologies), supplemented with half the concentration of the indicated cytokines. Infected cells were sorted 3 days post-transduction for use in downstream assays. HPC and HPC-5F were obtained according to (Doulatov et al., 2013). Infection was performed in StemSpan SFEM (StemCell Technologies) with 50 ng/ml SCF, 50 ng/ml FLT3, 50 ng/ml TPO, 50 ng/ml IL6, 10 ng/ml IL3 (all R&D Systems) and an MOI of 5-10 was used for the indicated constructs. Media was changed 24 hr post-infection and supplemented with doxycycline at 2 µg/ml (Sigma-Aldrich) to allow for the expression of the 5 factors. Prostate cancer cells (PC-3) and K562 cells were obtained from ATCC and cultured according to the suggested specifications. Cells were transduced with an MOI of 4-8 and media was changed 24 hr after infection. Cell were treated with Actinomycin D at 1 µg/ml (Sigma-Aldrich) for the indicated amount of time and then harvested.

Colony forming unit assays

1x10³ cells were plated into 3 ml of complete MethoCult (H4434; StemCell Technologies) and supplemented with 10 ng/ml FLT3, 10 ng/ml IL6, and 50 ng/ml TPO (all PeproTech). Colonies were scored manually after 14 days of incubation.

Mouse transplantation and assessment of human cell engraftment

NOD/LtSz-scidIL2Rgnull (NSG) (Jackson Labs) mice were bred and housed at the Boston Children's Hospital animal care facility, and experiments were performed in accordance to institutional guidelines approved by the BCH animal care committee. Briefly, 6-10 week old female mice were irradiated (275 rads) 24 hr before transplant. BM-transduced cells were GFP⁺ sorted 3 days post-infection. 7.5x10⁴ cells were transplanted per mouse in a 25 µl volume using a 28.5g insulin needle after temporarily sedating the animals with isoflurane. For HPC-5F transplantation experiments, cells were cultured for 14 days before injection, and 8x10⁶ cells were transplanted per mouse. For all the transplantation experiments, Sulfatrim was administered in drinking water to prevent infections after irradiation. Mice were sacrificed at the indicated time points. Injected femur, uninjected femur, and tibiae were collected and single cell suspensions were prepared using standard flushing and cell dissociation techniques. Samples were stained with a panel of human markers: CD19 PE (4G7; BD), CD45 PE-Cy5 (Immu19.2; Coulter), CD45 APC-Cy7 (2D1; BD), CD33 APC (P67.6; BD) and DAPI. Uninjected mouse bone marrow was used as a control for non-specific staining and BM mononuclear cells (Lonza) were used as a positive control for antibody staining, and proper compensation. All acquisitions were performed on a BD Fortessa cytometer.

Luciferase reporter assays

For the HMGA2-3'UTR reporter assay, 3'UTR sequences for the HMGA2-L (Rluc-3'UTRwt_HMGA2-L) and HMGA2-S (Rluc-3'UTRwt_HMGA2-S) isoforms were cloned into psiCHECK2 plasmid (which contains both Renilla [Rluc] and Firefly [Fluc] luciferases from Promega) downstream of the Renilla luciferase (Rluc) ORF. A mutant derivative of HMGA2-L 3'UTR mutated for all the miRNA binding sites of interest (Rluc-3'UTRmt_HMGA2-L) was synthesized (GeneScript). *Dgcr8* K/O MEFs (Novus Biologicals) were transfected along with miRIDIAN microRNA mimics using the DharmaFECT Duo reagent (Dharmacon). Rluc and Fluc activities were measured by Dual Luciferase assay (Promega) 72 hr after transfection. Ratios between Rluc and Fluc were calculated, and outliers of biological triplicates removed. To report HMGA2-L 3'UTR stability upon deletion of the miRNA sites, Rluc-3'UTRwt_HMGA2-L values were normalized to those of Rluc-3'UTRmt_HMGA2-L (set to the value of 100%), within the same miRNA treatment. To show which HMGA2 3'UTR isoform was more stable upon miRNA treatments, Rluc-3'UTRwt_HMGA2-L values were normalized to those of Rluc-3'UTRwt_HMGA2-S (set to the value of 100%), within the same miRNA treatment. For the splicing reporter assay, the genomic region of HMGA2-L exon 4 along with 500bp on either side (Luc-exon-4-WT) was cloned in between the splicing acceptor and donor sequence of a spliced Fluc ORF reporter plasmid (pcDNA3.1-Luc (Martone et al., 2016)). The mutant derivative of the SRSF1 site within exon 4 was generated by deleting its consensus motif.

Transfection of miRNA hairpin inhibitors

CD34⁺ cells isolated from CB were seeded at a density of 1.6x10⁵/well in a 12-well plate and pre-stimulated for 4 hr in StemSpan SFEM (StemCell Technologies) supplemented with FLT3, SCF, IL-6 and TPO, as indicated. miRIDIAN miRNA hairpin inhibitors

(Dharmacon) were transfected using DOTAP Liposomal Transfection Reagent (Sigma-Aldrich). After 24 hr, the media was replaced with fresh media and cells were harvested at 72 hr post-transfection.

METHOD DETAILS

RNA and DNA sequencing libraries

RNA was extracted from cells using the miRNeasy kit (QIAGEN). Transcriptional profiling of HSC and PROG populations and HPC-5F cells transduced with *CLK3/HMGA2* constructs was generated from 100 ng of total RNA for each biological replicate using the Tru-seq RNA Library Preparation Kit v2 (Illumina). Transcriptional profiles of BM-HSCs transduced with *CLK3* and *HMGA2*-S+3'UTRwt constructs was performed from 1-5 ng of total RNA using the SMART-Seq v4 Ultra Low Input RNA Kit (Clontech) in combination with the Nextera XT DNA Library Preparation Kit from 150 pg of cDNA (Illumina). ChIP-seq libraries were performed as previously described (Cacchiarelli et al., 2015) after immunoprecipitation with antibodies for V5 (MBL Int., Lot #5) and H3K4me2 (Diagenode). Libraries were sequenced on an Illumina HiSeq 2000 or 2500 according to protocol specifications.

miRNA profiling and analysis

For each biological replicate, 100 ng of RNA was utilized for miRNA profiling using the nCounter Human v2 miRNA Expression Assay (NanoString Technologies). Several steps were then undertaken to normalize the Nanostring data. First, Nanostring miRNA counts underwent QC and normalization according to manufacturer's specifications. The normalized counts were subsequently grouped and summed by their respective miRNA family. Then, for each sample, the expression of a given miRNA family was calculated as a percentage of the total counts for that sample (i.e., total measured miRNA content) in the Nanostring data. A two-sided unpaired t test was applied to compare the expression of each miRNA family across samples.

RNA-seq alignment and transcript assembly

RNA sequences were aligned using TopHat v2.0.14 (Trapnell et al., 2012) using default parameters. Sequences were aligned to the hg19 reference genome. For the HSC/PROG samples, Gencode v17 transcript annotation was used as the transcriptome index. For all other RNA-seq samples, Gencode v19 transcript annotations were used. For HPC-5F cells transduced with *CLK3/HMGA2* and for BM-HSCs transduced with *CLK3/HMGA2*-S+3'UTRwt, no novel junctions were considered (using the parameter “—no-novel-juncs”). Visualizations and Sashimi plots of RNA-seq alignments were performed using IGV v2.3 (Robinson et al., 2011).

Downstream transcript assembly and differential expression analysis were performed using Cufflinks v2.2.1 (Trapnell et al., 2012). For HSC/PROG samples, Cufflinks-assembled transcripts were merged with the Gencode v17 annotations using the Cuffcompare and Cuffmerge functions to generate a “Gencode v17 + Cufflinks” annotation file. Novel lincRNA discovery and annotation for Cufflinks-assembled transcripts was then performed according to Cabilli et al. (Cabilli et al., 2011).

For the HSC/PROG transcriptome profiling, aligned sequences were quantified using the Gencode v17 + Cufflinks annotation file using Cuffquant with default parameters. For the *CLK3* and *HMGA2* overexpression in BM-HSCs and HPC-5F cells, aligned sequences were quantified using Cuffquant with the Gencode v19 annotation file. Lastly, the Cuffnorm function was used to calculate expression in Fragments Per Kilobase of transcript per Million mapped reads (FPKM). A mask file was used during quantification for all datasets; this mask file was comprised of all rRNA, scRNA, snoRNA, snRNA, miRNA, “misc_RNA,” and tRNA sequences as annotated in Gencode v17 or v19. Unless otherwise noted, all Cufflinks default parameters were used.

Processed RNA-seq gene and isoform-level expression profiles for human hematopoietic cells from the cord blood lineage (n = 63 samples) were downloaded from the Blueprint Epigenome dataset (<http://www.blueprint-epigenome.eu>, downloaded on May 4, 2016).

We note that Gencode v17 and v19 annotate the *HMGA2*-S isoform (ENST00000393578) as being 316 bp in length. Newer versions of Gencode (e.g., v27) annotate it as 911 bp, which is consistent with the observed sequencing alignments and RT-PCR. As there are no competing exons near the *HMGA2*-S 3'UTR, using Gencode v17 or v19 does not substantially impact our quantifications or differential expression results.

Differential expression analyses, RT-PCR and qPCR

Differentially expressed genes and isoforms were identified using the Cuffdiff function within Cufflinks. All default parameters were used, and a mask file as described above was applied. For the HSC/PROG data, the Gencode v17 + Cufflinks annotation was used. For the *CLK3* and *HMGA2* overexpression in BM-HSCs and HPC-5F cells, the Gencode v19 annotation was used.

For the HSC and PROG data, specific filtering criteria were applied to generate a subset of differentially expressed genes/isoforms. For each pairwise comparison, significantly differentially expressed (FDR < 0.01) genes were identified. To define isoform-exclusive events, we identified significantly differentially expressed (FDR < 0.01) isoforms that are non-significant (FDR > 0.01) for their corresponding gene-level differential expression.

For the *CLK3/HMGA2* overexpression data in BM-HSCs, significantly differentially expressed genes were defined as showing absolute fold change > 2 relative to control, FPKM > 1 in either the overexpression or control sample, and FDR < 0.05.

FPKM values were plotted as the mean and standard deviation of the FPKM replicate mean values and when indicated, statistical significance was reported as the p value output by the Cuffdiff function.

Semiquantitative PCR was performed to validate isoform splicing and usage by direct amplification of the relevant exon-intron structures. To quantify full *HMGA2* mRNAs, PCR were performed on RNA-seq libraries (performed using polyA+ capture), amplifying the full coding sequence. To quantify *HMGA2* pre-mRNA, PCR was performed on cDNA reverse transcribed with random hexamers on polyA- RNA, amplifying a 5' portion of pre-mRNA. All PCR products were purified and run on a Bioanalyzer or TapeStation (Agilent Technologies) to obtain digital gels from electropherograms. In each sample, *HPRT1* was used as an endogenous housekeeping control. Virtual run traces are shown at global scale visualization adjusting brightness/contrast for best representation.

Quantitative PCR (qPCR) of mRNAs and miRNAs was performed using the miScript system (QIAGEN). Outliers of technical replicates were removed, and ΔCt or $\Delta\Delta\text{Ct}$ analyses were performed using *HPRT1* and *U6* as endogenous controls.

Definition of HSC transcriptional signatures

For HSC/PROG RNA-seq samples, significant isoforms and lincRNAs were defined as having expression of FPKM > 5 in at least one sample, an absolute fold change > 2 , and FDR < 0.05 in at least one pairwise comparison.

For HSC/PROG miRNA expression, normalized Nanostring expression data was used (see above). The mean values across sample replicates were used. miRNAs families were filtered for having an absolute fold change > 2 and a p value < 0.05 in at least one pairwise comparison and representing $> 0.1\%$ of total measured miRNA content.

To classify these significant isoforms, lincRNAs, and miRNAs into groups, the Jensen–Shannon divergence was calculated using the *csSpecificity* function implemented in *CummeRbund* (Trapnell et al., 2012). A specificity score > 0.25 was used to classify isoforms, and lincRNAs, and miRNAs as being enriched in a given sample and to define transcriptional signatures for each sample.

To generate a heatmap, the expression values were then z-score normalized, and the plotting order of isoforms, lincRNAs, or miRNAs were based on the specificity classifications. The *heatmap.2* function within the *gplots* package in R v3.1.1 was used to generate the heatmap.

Gene set enrichment analysis (GSEA)

GSEA were performed as previously described using curated gene sets available in MSigdb (Subramanian et al., 2005), or gene sets generated from HSC and PROG gene signatures (see above). Visualization of GSEA results was performed using *BubbleGum* (Spinellicci et al., 2015).

ChIP-Seq alignment and promoter analysis

Reads were aligned to the hg19 human genome using *Bowtie2* (Langmead and Salzberg, 2012) with default parameters. Enrichment at genomic 1kb tiles and promoters (defined as 1 kb up- and downstream of RefSeq transcription start sites) was computed by using the *Bedtools* “coverage” command to count the number of reads in tile or promoter region (Quinlan and Hall, 2010). Visualizations of ChIP-seq alignments were performed using *IGV* v2.3 (Robinson et al., 2011). In order to control for tiles or promoter regions with an over- or under- enrichment of reads due to technical artifacts such as low sequence complexity, the top 15% of regions with the most number of reads and the bottom 15% of regions with the fewest reads from the whole cell extract samples were discarded. The number of reads from sample replicates were summed to yield sample totals for each region.

Differentially-bound promoters were defined as those in which the number of both H3K4me2 and V5 reads were less than the 25th or greater than the 75th percentile in either *HMGA2-L* or *HMGA2-S* treatments. Differentially-expressed genes from the same samples were defined as those genes that were expressed at > 5 FPKM in any sample and showed at least an absolute 2-fold change in a comparison between two samples. RNA-seq and ChIP-seq results were then combined to study the relationship between *HMGA2* occupancy on expression. The median expression and median occupancy levels were used as cutoffs to separate the data into four quadrants.

let-7 target analysis

Data from TargetScan human version 7 was used to identify predicted conserved miRNA binding sites (www.targetscan.org). Predicted miRNA binding scores for all isoforms was kindly generated by George Bell (Whitehead Institute). The top 50% of *let-7* target isoforms were determined by having the lowest (i.e., strongest) weighted context++ scores. For target isoforms with more than one *let-7* binding site, the binding site with the strongest weighted context++ score was used. The mean expression of the *let-7* target isoforms for each sample (FL-HSC, CB-HSC, BM-HSC, FL-PROG, CB-PROG, BM-PROG, and HPC) was then calculated. The mean expressions were then z-score normalized for plotting.

PSI analysis

Percent-spliced-in (PSI) analysis was performed using *SUPPA* (Alamancos et al., 2015). Splicing events (alternative 5' splice site [A5], alternative 3' splice site [A3], alternative first exon [AF], alternative last exon [AL], mutually exclusive exon [MX], retained intron [RI], and skipping exon [SE]) were generated from the Gencode v19 annotation file or Gencode v17 + Cufflinks annotation file using default parameters. Input RNA-seq quantifications were based on the RNA-seq quantifications as described above, except FPKM expression values were converted to transcripts per kilobase million (TPM) as recommended by the software developers. Events were filtered for TPM > 1 . PSI calculations were then performed using the “psiPerEvent” tool. Differential splicing analysis was performed

using the “diffSplice” tool. Default parameters were used, and the “empirical” method was used to calculate significance. A p value threshold of 0.05 was used for declaring significance. Of note, the direction of dPSI for SE events was flipped from the software default to reflect actual splicing changes.

Splicing factor screen

To identify candidate splicing factors for *HMG A2* splicing, we applied several filters. We selected genes from the GO category “RNA binding” (GO:0003723). We then filtered for candidate genes that display an absolute fold change > 2 in FL-HSCs versus CB-HSCs and expressed at FPKM > 10 in either those samples. Among the filtered candidates genes, 23 genes available as lentiviral constructs from the Broad Institute Genome Perturbation Platform (GPP) were subsequently tested through overexpression in PC-3 cells.

Identification of SRSF1 binding motif

A search for SRSF1 binding sites was performed using the scanMotifGenomeWide function in HOMER (<http://homer.ucsd.edu/homer/motif/genomeWideMotifScan.html>) using the hg19 reference genome (Heinz et al., 2010). All software default parameters were used. The SRSF1 binding position-weighted matrix from (Wang et al., 2011) was used. A p value threshold of 1×10^{-8} was applied and only “+” strand hits were kept.

RNA binding protein enrichment

The PSI data from above was used to generate exons skipped (SE events) upon *CLK3* overexpression in BM-HSCs as compared to control. A p value threshold from the PSI analysis of 0.05 was used to identify exons that are preferentially increased or decreased upon *CLK3* overexpression. Background control exons were identified using exons with p value > 0.10. The rMAPS v1.0.6 online software (<http://rmaps.cecsresearch.org>) was used to perform the enrichment analysis (Park et al., 2016). All default parameters were used in the enrichment analysis, including the binding motifs provided by the software.

QUANTIFICATION AND STATISTICAL ANALYSIS

No statistical methods were used to predetermine sample size. In general, as descriptive statistics, we reported mean \pm SEM values with the exception of RNA-seq data where we reported mean \pm SD values. If not stated otherwise, t test (for two groups) or ANOVA (more than two groups) were the standard statistical tests applied. Pairing, repeated-measurements, or other test corrections were applied as needed. To assess statistical significance for CFU measurements, we applied analysis of deviance for generalized linear models (Chambers and Hastie, 1991). For *in vivo* engraftment capacity, the Mann-Whitney test was applied individually by comparing each treated sample with respect to the control sample.

DATA AND SOFTWARE AVAILABILITY

The accession number for the RNA-seq, ChIP-seq, and miRNA nanostring data reported in this paper is GEO: GSE109093.